*J. Fluid Mech.* (2007), *vol.* 589, *pp.* 479–507.  
doi:10.1017/S0022112007007884 Printed in the United Kingdom

# On the periodically excited plane turbulent mixing layer, emanating from a jagged partition

E. KIT[1], I. WYGNANSKI[1], D. FRIEDMAN[1], O. KRIVONOSOVA[2] AND D. ZHILENKO[2]

[1]Department of Fluid Mechanics and Heat Transfer, Faculty of Engineering
Tel-Aviv University, Tel-Aviv 69978, Israel
kit@eng.tau.ac.il

[2]Institute of Mechanics, Moscow State University, Michurinski pr., 1, Moscow, Russia

(Received 25 December 2006 and in revised form 15 June 2007)

The flow in a turbulent mixing layer resulting from two parallel different velocity streams, that were brought together downstream of a jagged partition was investigated experimentally. The trailing edge of the partition had a short triangular 'chevron' shape that could also oscillate up and down at a prescribed frequency, because it was hinged to the stationary part of the partition to form a flap (fliperon). The results obtained from this excitation were compared to the traditional results obtained by oscillating a two-dimensional fliperon. Detailed measurements of the mean flow and the coherent structures, in the periodically excited and spatially developing mixing layer, and its random constituents were carried out using hot-wire anemometry and stereo particle image velocimetry.

The prescribed spanwise wavelength of the chevron trailing edge generated coherent streamwise vortices while the periodic oscillation of this fliperon locked in-phase the large spanwise Kelvin–Helmholtz (K-H) rolls, therefore enabling the study of the interaction between the two. The two-dimensional periodic excitation increases the strength of the spanwise rolls by increasing their size and their circulation, which depends on the input amplitude and frequency. The streamwise vortices generated by the jagged trailing edge distort and bend the primary K-H rolls. The present investigation endeavours to study the distortions of each mode as a consequence of their mutual interaction. Even the mean flow provides evidence for the local bulging of the large spanwise rolls because the integral width (the momentum thickness, $\theta$), undulates along the span. The lateral location of the centre of the ensuing mixing layer (the location where the mean velocity is the arithmetic average of the two streams, $y_0$), also suggests that these vortices are bent. Phase-locked and ensemble-averaged measurements provide more detailed information about the bending and bulging of the large eddies that ensue downstream of the oscillating chevron fliperon. The experiments were carried out at low speeds, but at sufficiently high Reynolds number to ensure naturally turbulent flow.

## 1. Introduction

When two parallel streams of different species or velocities merge at the end of a flow partition, they create a mixing layer that spreads-out approximately linearly in the direction of streaming after passing through an initial adjustment length. This length is sensitive to the state of the boundary layers that develop over the splitter plate (their thickness and whether they are laminar or turbulent) and to the velocity

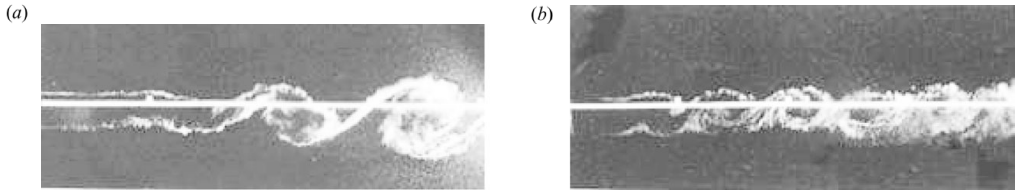


FIGURE 1. Periodically excited, plane turbulent mixing layer generated between two parallel streams (reproduced from Oster *et al.* 1978).

and density ratio between the streams. When the velocity ratio is large and the boundary layers are thin the adjustment length is short. Nevertheless, the streamwise streaks existing in the upstream, turbulent boundary layers and in the wake created downstream of the flow partition, introduce inflow conditions that are foreign to the 'ideal' mixing layer. It is always a challenge to separate the auspicious factors entering the region of interest, from the natural perturbations in the flow that emerge from the instabilities evolving under ideal conditions. Such may be the case with some observations related to streamwise streaks in mixing layers.

The characteristics of the turbulent large-spanwise-structures in a plane periodically excited mixing layer have been extensively investigated for over a quarter of a century. These investigations proved that there is considerable order within the apparent chaos that is synonymous with turbulence. Most of the orderly travelling structures represent concentrations of spanwise vorticity that are associated with the Kelvin–Helmholtz instability mechanism (e.g. Gaster, Kit & Wygnanski 1985; Cohen & Wygnanski 1987). Therefore these structures can be enhanced and manipulated by periodic perturbations that excite the mean flow whose width is commensurate with the wavelength of the excitation. Even a very weak plane harmonic disturbance can change the mean spreading rate of the flow by increasing the growth of its spanwise rolls (Oster *et al.* 1978). The sole difference in figures 1(*a*) and 1(*b*), in which a mixing layer is visualized by smoke, is the frequency of the excitation which is twice as high in figure 1(*b*). It is clear that the eddy size and the corresponding width of the mean flow are quite different in the two photographs.

The dimensionless spreading rate of a mixing layer that had been excited by a plane wave emanating from the trailing edge of a solid partition or nozzle can be divided into three regions. The portion of the mixing layer adjacent to the excitation (Region I of figure 2) diverges, principally as a result of the amplification of quasi-two-dimensional waves. Region II starts where the mixing layer ceases to grow because it is neutrally stable to the imposed harmonic disturbances that dominate the flow. This occurs at a Strouhal number $\theta^+ = \theta f_e/\overline{U} \approx 0.075$ (where $\theta$ is momentum thickness, $\overline{U} = (U_1 + U_2)/2$ is the average velocity and $U_1$ and $U_2$ are the velocities of the two streams and $f_e$ is the excitation frequency). The location underlying the onset of neutral stability is thus proportional to the frequency of the excitation. This onset is associated with the 'roll-up' of the excited instability wave into a discrete vortex and if other frequencies are also present, vortex amalgamation (usually pairing) may be observed. Wherever a single frequency dominates the flow, Region II extends over the approximate range $1 < Rf^+ < 2$, where $f^+ = fx/\overline{U} = x/\lambda_x$ represents a dimensionless distance measured in terms of the number of streamwise wavelengths $\lambda_x$ that it contains. Similarly, $\theta^+ = f\theta/\overline{U} = \theta/\lambda_x$ represents a dimensionless momentum thickness $\theta$ measured relative to the streamwise wavelength. $R = (U_1 - U_2)/(U_1 + U_2)$ may be regarded as the ratio between the typical vorticity of a large spanwise

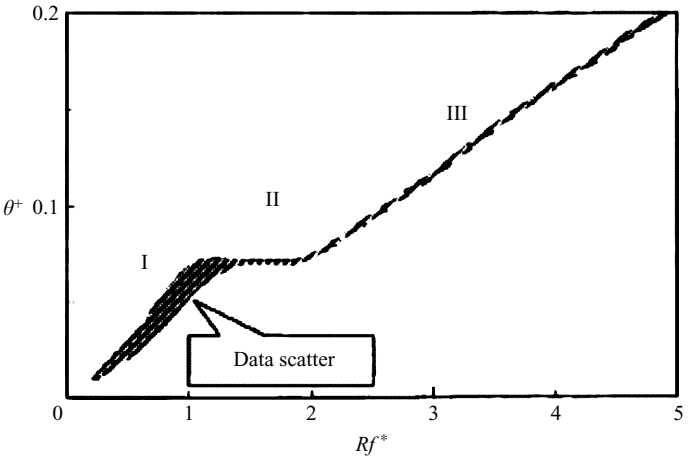


FIGURE 2. Dimensionless spreading rate of a mixing layer subjected to periodic excitation (reproduced from Wygnanski & Petersen 1987).

eddy, $(\Delta U/L)$, and the frequency of its appearance (i.e. the advection velocity $U_\varphi$ of the eddy divided by its characteristic size $U_\varphi/L \propto [U_1 + U_2]/L$), which consequently indicates the angle of rotation of the large spanwise vortex during the eddy period. In the above expression $\Delta U$ is velocity difference between the two streams and $L$ is the characteristic length of the problem, streamwise wavelength $\lambda_x$ divided by $2\pi$ is selected as suggested by Gaster *et al.* (1985). The above ratio is thus representative of the strength of the spanwise eddies. Beyond $Rf^+ \approx 2$, the coherent Reynolds stresses (associated with the excitation frequency) lose their relative significance and the mixing layer continues to spread out linearly (Region III) with increasing distance from the splitter plate.

The dominance and perseverance of the large spanwise rolls (Wygnanski *et al.* 1979, Browand & Ho 1983) suggests that most of the momentum transfer in Regions I and II could be accounted for by assuming that the flow is two-dimensional. If the remaining incoherent (turbulent) motion is not only random but it is also fine scale, it may be represented by a simple eddy-viscosity model (Reau & Tumin 2002; Marasli, Champagne & Wygnanski 1991) that enabled Reau & Tumin (2002) to predict the changes in the rate of spread of the flow and the associated coherent Reynolds stresses resulting from the excitation. It does not consider any inflow effects, such as the coalescence of the boundary layers from both sides of the splitter plate, nor does it consider the possible coherence of the streamwise streaks that ride on the spanwise structures and are stretched by the strain field existing between adjacent rolls. Shadowgraph pictures of Konrad (1976) revealed the existence of the streamwise streaks whose spanwise spacing increases with increasing distance from the splitter plate. This spacing seems to scale with the local width of the flow, suggesting that the streaks are a product of a genuine instability of the mixing layer and not simply a testimony to imperfections on the surface of the splitter plate, or possibly wall streaks generated in its turbulent boundary layers.

There are various instability mechanisms that could generate streamwise streaks in a plane mixing layer. They can be a product of weakly nonlinear instability (Stuart 1967), they can also be generated by a triad wave interaction between two spanwise travelling modes and a streamwise mode (Craik 1971), or they can result from a secondary three-dimensional instability of the primary spanwise modes (Pierrehumbert &

Widnall 1982). Numerical simulations (Riley & Metcalfe 1980; Buell & Mansour 1989) also predict the existence of streaks that are associated with counter-rotating streamwise rib vortices that are stretched and strengthened in the vortex sheets (braids) that connect neighbouring spanwise rolls. Ho & Huerre (1984) gives a more detailed discussion of this phenomenon; however, the nature of the dominant mechanism responsible for the generation of the streamwise streaks (rib vortices) and their interaction with the spanwise eddies in the plane turbulent mixing layer is still not fully understood.

An important question concerning the development of a turbulent mixing layer is the mechanism of its transition to small-scale three-dimensional turbulence. In the vicinity of the splitter plate, the mixing layer forms two-dimensional Kelvin–Helmholtz (K-H) rolls that represent the primary instability of this free shear flow which does not vary along the span. Naturally created K-H rolls have a variety of sizes and therefore no dominant wavenumber. One way to regulate their wavenumber is by introducing small-amplitude two-dimensional oscillations into the flow (Gaster *et al.* 1985), but such excitation, more often than not, also affects the evolution of the turbulent mixing layer in the direction of streaming (e.g. Oster *et al.* 1978; Ho & Huerre 1984). Although these two-dimensional rolls persevere over long distances (Wygnanski *et al.* 1979; Browand & Troutt 1980), they are unstable, and they are susceptible to rapidly amplifying three-dimensional instabilities. The development of three-dimensional motions in a plane mixing layer was studied by Bernal & Roshko (1986) through flow visualization in water. They suggested that the secondary streamwise vortices are simply portions of a warped vortex that threads its way up and down between adjacent spanwise vortices, thus changing its streamwise directional sign on each pass. Similar observations were made by Lasheras & Choi (1988). These investigators enhanced and regulated the streamwise structures by corrugating the partition separating the two streams or by indenting its trailing edge in a sinusoidal manner. This procedure enabled them to control the initial spanwise wavelength of the streaks and to observe their intensification in the direction of streaming. Since they did not excite the flow periodically, they had no control over the spanwise rolls which consisted of a fairly broad spectrum that naturally underwent an amplification process. As a consequence, they were unable to determine uniquely the most unstable wavelength ratio of the two structures, stating only that it is in the range of 0.2 to 3 times the Kelvin–Helmholtz wavelength. It may also explain the apparent initial independence in the evolution of the two types of coherent structures. In order to encourage the interactions between them, Lacheras & Choi resorted to creating a weak non-uniformity in the flow and concluded that the 'streamwise streaks' are strain-related vortex tubes because they are aligned with the strain field and not with the free stream. Under the non-uniform flow conditions, an interaction was observed between the rolls and the streaks. Pairing of the primary spanwise vortices tangled further the counter-rotating longitudinal vortex streaks, possibly leading to the generation of small-scale vorticity and enhanced mixing. Since the frequency content of the rolls is not unique, the visual observation of pairing might correspond to the 'roll-up' of a larger wave on which a finite number of K-H rolls are riding (Wygnanski & Peterson 1985). Bell & Metha (1992) used cross-wire probes to measure the mean streamwise component of vorticity in a mixing layer that had regular spanwise perturbations imposed at its origin. Once again, the streamwise vortical structures were clearly related to the spanwise perturbations imposed on the flow.

Experimental investigations of streamwise vortices were carried out in a forced plane mixing layer by Huang & Ho (1990), Tung & Kleis (1996) and Leboeuf & Mehta (1996), where the flow field was acoustically excited by two frequencies: a fundamental

and its first subharmonic. No additional spanwise forcing was applied and hot-wire anemometry was used to conduct the measurements of the velocity and vorticity. This subsequently resulted in the phase-locked and ensemble-averaged spanwise and streamwise vorticity components that were computed to study the evolution of coherent primary and secondary vortical structures. Nygaard & Glezer (1990, 1991) were able to excite the spanwise rolls and the streamwise streaks in a time-dependent manner in water, by embedding heating elements in the splitter plate separating the two streams. Their method enabled an independent control of the spanwise and streamwise wavelengths. Hot-film anemometry was used for the velocity/vorticity measurements while a schlieren technique enabled them to carry out flow visualization. The streamwise streaks observed had a 'Λ' shape and they appeared first near the high-speed edge of the primary spanwise wave before it rolled up into a vortex.

There are also a number of theoretical and numerical studies pertaining to the development of three-dimensional vortical structures in the mixing layer. The computations consider homogeneous and stratified mixing layers. Pierrehumbert & Widnall (1982) identified two main classes of instability in their analysis of a shear flow, modelled by an array of Stuart vortices. The first class corresponded to localized pairing of vortex tubes that resulted in perturbations that varied along the span. The second class corresponded to so-called 'translative' instability and its most unstable mode had a spanwise wavelength that was equal to 2/3 of the streamwise wavelength, although the frequency band of the unstable modes was very wide. The DNS (direct numerical simulations) of a temporally growing mixing layer performed by Metcalfe *et al.* (1987) showed that spanwise instability modes lead to the formation of pairs of counter-rotating streamwise vortices in the braids connecting adjacent spanwise rolls. To model the development of the rib vortices (streamwise vortices in the braid region), Lin & Corcos (1984) computed the evolution of a vortex array, which had a sinusoidal distribution in a spanwise direction that was being stretched along its axis by a plane strain.

Rogers & Moser (1992) conducted numerical simulations of a three-dimensional temporally evolving plane mixing layer, showing how the spanwise vorticity rolled up into corrugated spanwise rolls, with streamwise rib vortices being developed in the braid region connecting these rolls. However, under certain initial conditions, persistent rib vortices did not develop, delaying the development of significant three-dimensionality in the flow. A new mechanism of small-scale transition via core dynamic instability, (CDI), which does not rely on rib vortices was studied numerically by Schoppa, Hussain & Metcalfe (1995). They showed that in the case of a bulging mode, which occurs when the three-dimensional perturbations generated on the partition are antisymmetric relative to the primary rolls, a rapid high-amplitude standing-wave oscillation of the roll's core size occurs without the need to form traditional ribs. It follows from the above, that the generation of different three-dimensional coherent structures is essentially dependent on the inflow conditions originating in the vicinity of the trailing edge of the splitter plate.

There is an increased interest in the interaction of between spanwise and streamwise vortices in aerodynamics and in aeroacoustics. The flow behind lambda (Λ) wings (e.g. the B-2 bomber) results in a mixing layer that alters the wing loading, whereas 'chevron' nozzles (figure 3) proved to be effective noise abating devices (E. Gutmark 2006). Thus far, personal communication the shapes of these nozzles or wing trailing edges have been empirically established, but the need for a better understanding of the process has emerged. There are other applications where spanwise and streamwise vortices interact and such interaction may dominate the mean flow. For example, in a wall jet flowing over a convex surface, there is an interaction between the K-H

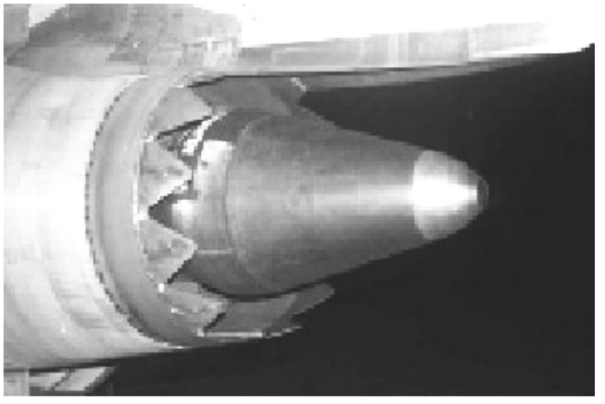

FIGURE 3. Chevron type nozzle in GE CF6 engine (from E. Gutmark, personal communication 2006).

spanwise rolls and streamwise vortices that are generated by a centrifugal instability. In this case at least, the origin of the streamwise vortices is understood, but not the ensuing interaction with the spanwise rolls.

Although spatial evolution of three-dimensional instabilities in free shear layers has been intensively studied, the appearance of vortex streaks and their dependence on the type of excitation is still not well understood. In particular, whether these streaks originate from the large spanwise rolls by a 'translative' instability as Pierrehumbert & Widnall (1982) have suggested, or from rib vortices generated and enhanced in the braid region. Further experimental study of the three-dimensional transition within the K-H rolls or between them, including especially designed non-uniform spanwise excitation of the mixing layer, is thus desirable. Attaching an oscillatory chevron-shaped fliperon to a stationary partition, generates spanwise rolls that periodically bulge along the span, and pairs of counter-rotating streamwise vortices whose relative intensity is affected by the shape and size of the chevron fliperon and by the fliperon's excursions.

The present investigation focuses on the behaviour and mutual interaction of these vortices in order to expose their combined effect on the mean flow and turbulence fields. A study of this interaction requires detailed three-dimensional mapping of velocities within the K-H billows and their evolution in space and in time. Conventional experimental tools can provide either high temporal resolution at a limited number of locations or high spatial resolution at a given instant. Since hot wires were mostly used to map the three-dimensional coherent structures in mixing layers, the spatial resolution of the available information is limited although a fairly large number of fixed locations were examined by cross-wires. Stereo particle image velocimetry (SPIV) was also employed to obtain velocity patterns along the mixing layer as well as in the crossflow plane at a given time. Periodic excitation provided a time reference that enabled the data acquired by SPIV to be phase locked to the excitation, thus relieving somewhat the shortcoming of its poor temporal resolution; it also provided a phase reference for extracting information about coherent structures whenever hot-wire anemometers were used. The experiments were carried out in the Tel Aviv mixing-layer facility that was constructed by Oster *et al.* (1978) and has been almost continuously used ever since (Gaster *et al.* 1985; Weisbrot & Wygnanski 1988; Zhou & Wygnanski 2001). It was slightly modified to accommodate a chevron-type oscillating fliperon and the optical quality of its sidewalls was improved. The respective velocities of each of the streams forming the mixing layer was 5 and $2\,\mathrm{m\,s^{-1}}$.

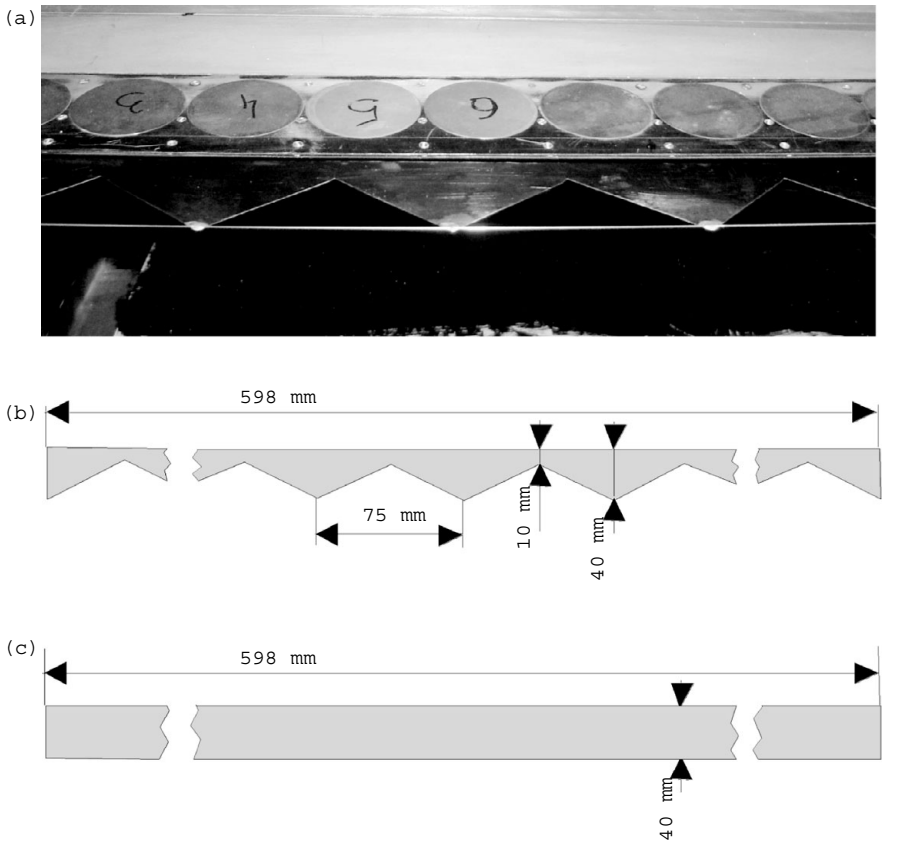


FIGURE 4. Layout of two- and three-dimensional fliperons: (*a*) photograph of a section of three-dimensional fliperon, (*b*) schematic diagram of three-dimensional fliperon, (*c*) schematic diagram of two-dimensional fliperon.

## 2. Experimental apparatus and measuring techniques

A detailed description of the apparatus is given by Oster & Wygnanski (1982). The new test section was 2000 mm long with crossflow dimensions of $500 \times 600\,\text{mm}^2$ throughout. The mixing layer was generated in the test section through the merger of two parallel streams created independently by the two cascade wind tunnels. The co-ordinate system is defined as follows: the distance from the splitter plate in the direction of streaming is $x$, the coordinate normal to the two streams forming the mixing layer is $y$ and the spanwise coordinate along the splitter plate is $z$. All distances have been rendered dimensionless by using the respective wavelengths $\lambda_x$, $\lambda_z$ and momentum thickness $\theta$ to normalize the streamwise $x$, spanwise $z$ and the lateral $y$ coordinates, respectively, thus: $\xi = x/\lambda_x$, $\zeta = z/\lambda_z$ and $\eta = (y - y_0)/2\theta$.

Two fliperons were alternately used in this experiment. They were both hinged to the trailing edge of the splitter plate and uniformly oscillated up to a maximum amplitude of 3 mm. They were driven by two electromagnetic shakers that displaced a piano wire to which the fliperon was attached (figure 4). The uniformity of the fliperon's oscillations was checked visually using stroboscopic lighting. The shaker was actuated by a controlled sinusoidal signal, generated by Labview software through a digital to analogue converter. One fliperon had a constant chord of 40 mm which provided

uniform oscillations along the span while the other had a triangular 'chevron' shape that was tied to a taught wire to ensure uniform amplitude of oscillations across the span. It had a chord that varied linearly between 10 and 40 mm over a spanwise distance of 37.5 mm, creating a spanwise wave of $\lambda_z = 75$ mm in length.

Three sets of periodically excited data are discussed in the present paper. They were mostly acquired at a single frequency of excitation, $f_e = 20$ Hz. A few experiments were carried out at other frequencies of $f_e = 30$ Hz and $f_e = 40$ Hz. Forcing the fliperons to oscillate at a single frequency of 20 Hz has a major effect on the rate of spread of the flow. The maximum excursions of the tip of the fliperon, amplitude $A$, were kept constant throughout each experiment. '$A$' was 1.5 mm in the two-dimensional experiments and was both 1.5 mm and 3 mm when the chevron-shaped fliperon was used. The larger amplitude was chosen in order to impart a similar overall perturbation amplitude to the flow with both types of fliperon, the chevron type requiring $A \approx 3$ mm whereas the two-dimensional type provided a similar average input at $A = 1.5$ mm. This provided an initial (measured at $x = 50$ mm) mean coherent disturbance level of normal velocity, of approximately 0.9% of $\Delta U$. To obtain this number, the phase-locked and ensemble-averaged streamwise velocity perturbations were integrated across the flow at various spanwise locations, they were averaged and then divided by the width of the mixing layer and velocity difference, $\Delta U = (U_1 - U_2)$. The two merging streams were maintained at velocities of 2 and 5 m s$^{-1}$ (i.e. at $R = (U_1 - U_2)/(U_1 + U_2) = 0.429$), resulting in a forced streamwise wavelength of $\lambda_x = 175$ mm at the perturbation frequency of 20 Hz which happened also to be the ratio between spanwise and streamwise wavelengths $\lambda_z/\lambda_x = 0.429$. Hot-wire measurements were made across the flow starting at $x = 50$ mm from the trailing edge of the partition and terminating at $x = 1000$ mm, thus encompassing about 50% of the 2 m long test section.

Two components of velocity were measured simultaneously at two spanwise locations across the mixing layer in order to establish the spanwise coherence of the motion. One probe was located at the centre of the mixing layer whereas the other could traverse in the $z$-direction. When the moving probe (probe 1) was not traversing, it was located opposite the shortest chord of the 'chevron' fliperon (dubbed as the notch) while the fixed probe (probe 2) was located opposite the largest chord of the fliperon (dubbed as the cusp).

The instantaneous velocity component, $q$, was decomposed into a temporal average quantity, $Q$, a phase-locked fluctuation $\langle q \rangle$ and the random residue $q_{rand} = q'$ (i.e. $q = Q + \langle q \rangle + q_{rand}$ which corresponds to triple decomposition, e.g. Hussain 1983). The phase locking was related to the periodic excitation signal imparted to the fliperon.

The coherent portion of the motion may be smeared-out by jitter due to variations in the free-stream velocity, the excitation amplitude and other random disturbances. They may therefore be poorly represented by a phase-locked and ensemble-averaged quantity (Zhou, Heine & Wygnanski 1996); however, the phase jitter of the dominant structures in the present flow was quite small. The coherent Reynolds stresses obtained from simple double decomposition of the motion and from phase-locked data, suggest that most of the Reynolds stress in Region I is coherent and therefore could not have a significant jitter. Consequently, only the conventional phase-locked and ensemble-averaged results are presented for the hot-wire data. Various aspects of the coherent motions, including phase-locked Reynolds stress, phase and amplitude distributions of the individual components of the disturbances and coherent vorticity contours were calculated from the measurements. Based on these results, the relation between coherent spanwise and streamwise structures and the growth of the mixing layer was observed.

SPIV provided data of all three velocity components of velocity. The SPIV system contained a Nd:YAG double-pulse laser with light beams of 532 nm wavelength, receiving optics, and two 'Kodak' cameras having a $1012 \times 1008$ pixel resolution. A theatrical fog-machine (Antari, model Z-1200) generated particles having a mean diameter of approximately 1–2 μm, which were used for seeding the flow. The physical size of the measured images was $220 \times 150\,\mathrm{mm}^2$. Most images were obtained in the crossflow $(y, z)$-plane. The interrogation area varied from $24 \times 24$ up to $48 \times 48$ pixels, and was used to generate $100 \times 80$ velocity vector calculations employing IDT provisional software. In most of the experiments presented, the $24 \times 24$ pixel interrogation area was used. The IDT software provides a subpixel resolution of about 0.1, so the estimated accuracy of the ensemble-averaged velocity vectors is about 1% for $u$, 3% for $v$ and 5.7% for $w$. Images were aquired in two different modes. In the random-phase mode, the acquisition was carried out using an internal clock. These images were obtained in an arbitrary way relative to the controlled sinusoidal oscillation of the fliperon, and were therefore also randomly phased relative to the K-H structures in the mixing layer. In the phase-locked mode, measured images were obtained with prescribed time shifts relative to the controlled excitation signal and the K-H structures. At each phase, the measurements were repeated 400 times to provide a large enough ensemble of raw data. After the series of images were ensemble averaged, mean velocity vectors were obtained in the first mode of operation and the phase-averaged velocity vectors in the second.

Constant-temperature hot-wire (HW) anemometers (AA Lab Systems) were used to measure the $u$ and $v$ components of velocity throughout the flow field and provided a direct comparison with the two-dimensional excited mixing layer. Measurements of the third component, $w$, were temporarily postponed awaiting a detailed investigation of the specific modal interaction between the two types of vortices that is planned in the future. Two hot-wire probes were used for velocity measurements: one had two degrees of freedom and was able to move in the $x$ and $y$ directions, whereas the other had three degrees of freedom and could move in the $x$, $y$ and $z$ directions, with distance resolution of 0.01 mm. The signals from the sensors that were sampled at rates of 2000 or 4000 samples $\mathrm{s}^{-1}$ per channel, were converted to velocities using a standard calibration procedure (e.g. Weisbrot & Wygnanski 1988), and were stored for further processing.

At the first stage of the processing, the local mean velocity at each measuring point was computed by averaging the entire record, whose duration exceeded 100 excitation periods and it was subtracted from the raw signal. Further decomposition of each velocity component to the coherent and random parts was conducted using the excitation signal for phase reference. The number of points so analysed at any one of three cross $(Y–Z)$ planes was $2091 = 51 \times 41$, for lateral $y$ and spanwise $z$ coordinates correspondingly.

## 3. Results and discussion

### 3.1. *The mean flow*

The mean centre of a turbulent two-dimensional mixing layer is arbitrarily defined by the lateral location $y_0$ (e.g. Gaster *et al.* 1985). With some reservation, the values of $y_0$ represent the lateral locations of the centres of the large spanwise rolls and enable us to assess their distortion or bend. The distribution of $y_0$ is presented in figure 5. In the absence of periodic excitation, $\mathrm{d}y_0/\mathrm{d}x = \text{constant}$ at all distances from the splitter plate and is therefore represented by a straight line in figure 5(*a*). Plane periodic excitation results in an earlier roll-up of the large transverse rolls and thus

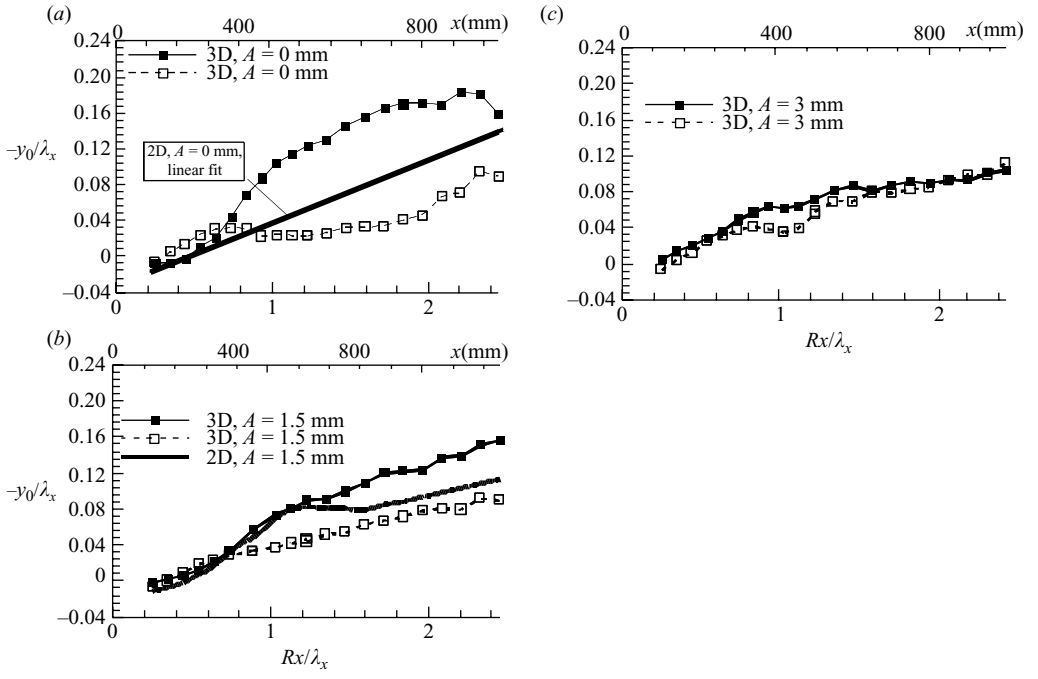


FIGURE 5. Normalized distribution of the mean centre location, $(y_0/\lambda_x)$, of the mixing layer. ■, fliperon notch; □, fliperon cusp.

larger initial values of $\mathrm{d}y_0/\mathrm{d}x$ that is followed by saturation ($\mathrm{d}y_0/\mathrm{d}x \approx 0$) associated with the neutrally stable and decaying modes of the externally excited eddies. Since these relationships have been extensively discussed in the past (e.g. Wygnanski & Peterson 1985) the two-dimensional data are represented by a curve fit for the sake of comparison only.

The initial three-dimensional perturbations generated by the stationary chevron fliperon, resulted in the most significant bending of the spanwise rolls starting at $Rx/\lambda_x > 0.7$. The bend increased monotonically until $Rx/\lambda_x = 1.8$ where the difference between the location of $y_0$ opposite the notch and the cusp in the fliperon was $0.13\lambda_x$. This distance is commensurate with the depth of the notch, but more surprising is the perseverance of the distortion in the direction of streaming that exceeded $10\lambda_z$. Little wonder that a chevron nozzle has such a large impact on the turbulent structure of the jet and its associated noise.

With the chevron fliperon oscillating at an amplitude of 1.5 mm, the inferred spanwise bending became considerably weaker. It started being noticeable only at $Rx/\lambda_x > 0.7$ and it increased in the direction of streaming. Nevertheless at $Rx/\lambda_x = 1.8$ it represented less than a third of the distortion existing in the absence of the imposed oscillations. When the initial perturbation amplitude was increased to 3 mm, the variations of $y_0$ with $z$ were virtually eliminated (figure 5*c*), suggesting that the oscillations of the chevron fliperon inhibit the bending of the large spanwise rolls. $(\mathrm{d}y_0/\mathrm{d}x)$ of this highly perturbed three-dimensional mixing layer is not much different from the two-dimensional unperturbed flows as long as $Rx/\lambda_x < 1.4$; farther downstream $(\mathrm{d}y_0/\mathrm{d}x)$ is very small, reminiscent of the highly perturbed two-dimensional flow.

An integral length scale $\theta = \theta(z)$ defines the local width of the flow regardless of its dimensionality or the presence of kinks in its local mean velocity profile. It is often

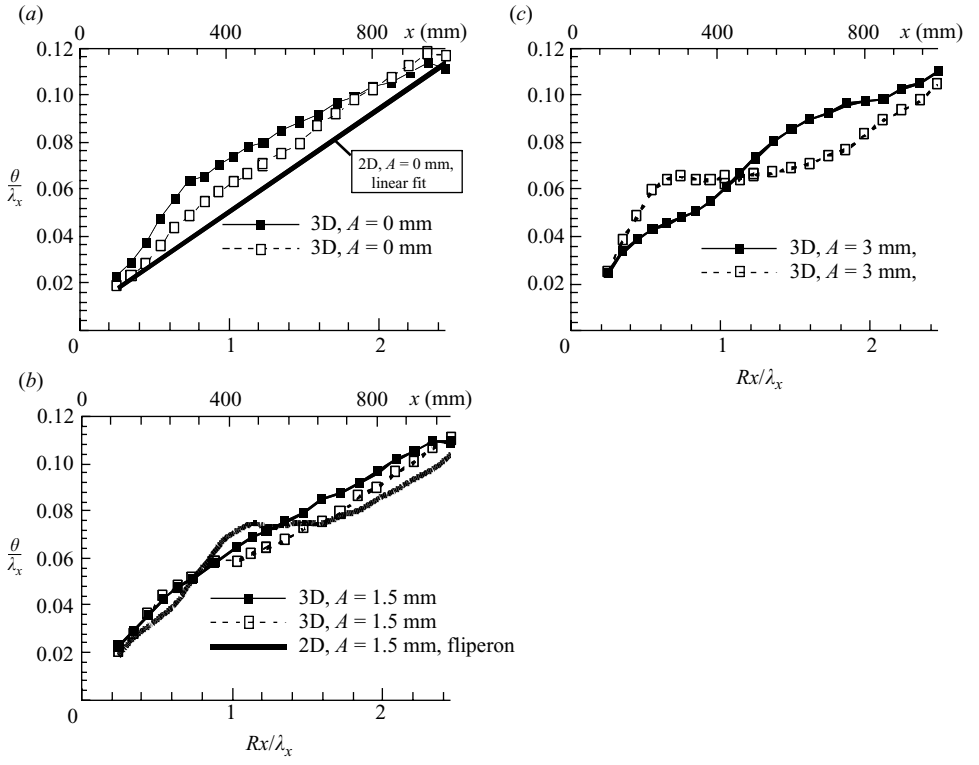


FIGURE 6. Momentum thickness ($\theta$) distribution along the mixing layer. ■, fliperon notch; □, fliperon cusp.

referred to as the momentum thickness, although it does not represent a deficit in momentum as we know it from boundary-layer theory. It is defined as:

$$\theta = \int_{-\infty}^{\infty} \frac{U - U_2}{U_1 - U_2} \left[1 - \frac{U - U_2}{U_1 - U_2}\right] \mathrm{d}y.$$

The increase of momentum thickness in the direction of streaming is shown in figure 6 for the two spanwise locations: one opposite the cusp in the chevron fliperon and the other opposite the notch. The increase of momentum thickness when the fliperon was stationary is shown in figure 6(*a*). When the plane fliperon was used, the velocity distributions measured by both probes were almost identical indicating again that the flow is two-dimensional. The two-dimensional fliperon in the absence of excitation generates a traditional two-dimensional mixing layer, whose spreading rate, $(\mathrm{d}\theta/\mathrm{d}x)$, is practically constant over the entire range of measurement. The momentum thickness for the stationary chevron fliperon, measured by the probe placed opposite its cusp (see figure 6*a*) was somewhat smaller than opposite its notch. We may not attribute the difference in $\theta$ to the effective distance from the fliperon which is larger when measured from the notch than from the cusp, because any attempt to superpose the two curves requires a movement in $x$ that exceeds the depth of the notch by a factor of 3. The mixing layer downstream of a passive chevron fliperon diverges initially at a higher rate than the two-dimensional mixing layer with $0.03 < (\mathrm{d}\theta/\mathrm{d}x) < 0.037$ where the higher value corresponds to the probe located opposite the trough (notch) in the fliperon. At $Rx/\lambda_x > 0.7$, $(\mathrm{d}\theta/\mathrm{d}x)$ is abruptly reduced to $0.014 < (\mathrm{d}\theta/\mathrm{d}x) < 0.018$ with the location of the higher $\mathrm{d}\theta/\mathrm{d}x$ switching over to the cusp in the fliperon. The passive

chevron fliperon increases the local width of the flow throughout the domain of measurement owing to the large initial increase in $\mathrm{d}\theta/\mathrm{d}x$. Both base-flow distributions of $\theta$ are larger downstream of the three-dimensional fliperon than of the two-dimensional fliperon.

Oscillating the chevron fliperon at $A = 1.5$ mm evened out the irregularities of the thickness between the flow downstream of the notch and the cusp, provided $Rx/\lambda_x < 0.7$ (figure 6*b*). Since in this region $y_0$ was also independent of $z$ (figure 5*b*), it implies that this level of excitation by the chevron fliperon not only straightened the large spanwise eddies, but also evened out their size. At $Rx/\lambda_x > 0.7$, the large eddies opposite the cusp stayed closer to the high-speed stream and their local width $\theta$, was also smaller, when compared to the eddies that were downstream of the notch.

The active two-dimensional fliperon oscillating at $A = 1.5$ mm, increases the divergence of the mixing layer in Region I (see Oster *et al.* 1978; Oster & Wygnanski 1982) to $\mathrm{d}\theta/\mathrm{d}x = 0.0325$, (figure 6*b*), that is still lower than the $\mathrm{d}\theta/\mathrm{d}x$ provided by the passive chevron opposite its notch. At $Rx/\lambda_x = 1$ (corresponding to $x = 400$ mm), $\mathrm{d}\theta/\mathrm{d}x = 0$ and the flow enters Region II after the neutral value of $f_e\theta/\bar{U} = 0.075$ is reached. The almost parallel flow region terminates around $Rx/\lambda_x = 1.7$ whereupon the mixing layer resumes its unexcited rate of spread. The stepwise rate of spread represents the classical behaviour of the turbulent mixing layer that was excited by plane periodic oscillations. A similar plateau in which $\mathrm{d}\theta/\mathrm{d}x = 0$ is observed opposite the cusp of the chevron fliperon that oscillated at an amplitude, $A = 3$ mm; however, the neutral value of $f_e\theta/U_c = 0.064$ is lower and it occurs at a shorter distance from the fliperon ($Rx/\lambda_x = 0.7$). The chevron fliperon imparts a much smaller perturbation to the flow downstream of the notch and consequently $\mathrm{d}\theta/\mathrm{d}x$ opposite the notch is much smaller (figure 6*c*). While $\mathrm{d}\theta/\mathrm{d}x = 0$ opposite the cusp, $\mathrm{d}\theta/\mathrm{d}x$ was reduced opposite the notch although $\theta$ was much smaller than the value required for plane saturation at this distance from the fliperon.

The dimensional momentum thickness $\theta_0$ at separation was computed by extrapolating the $\theta$-plots (figure 6) to the origin as suggested by Browand & Latigo (1979). It yielded $\theta_0 = 0.5$ mm resulting in $\lambda x/R\theta_0 = 815$. The Reynolds number based on this hypothetical thickness, $\theta_0$, was: $Re(\theta_0) = 90$. It is high enough to allow rapid amplification of perturbations introduced by the oscillating fliperon as was shown by Gelfgat & Kit (2006). According to their figure 15, K-H instability develops rapidly whenever $Re(\theta_0) > 20$. Since the flow phenomena described in this study occur at distances where the mixing-layer width (described by local $\theta$) is an order of magnitude larger than it is at the origin of the flow, the detailed knowledge of the initial $\theta_i$ is of little significance.

The initial evolution of the flow downstream of the chevron fliperon that oscillated at an amplitude of only 1.5 mm was quite different from $A = 3$ mm. At $A = 3$ mm, the local thickness of the mixing layer varied along the span while its lateral displacement did not. At $A = 1.5$ mm, the lateral displacement still varied along the span while the thickness did not. We may infer from these results that $A = 3$ mm resulted in local bulging of the large eddies because of the amplitude differential imparted to the flow by the harmonic excitation of the chevron fliperon, while the large eddies associated with the $A = 1.5$ mm excitation were initially even along the span, but they were dislocated in the lateral direction, i.e. they were bent.

A sketch that outlines different modes of possible three-dimensional perturbations is drawn in figure 7 (see also Schoppa *et al.* 1995). When the rib vortices, developed by strong undulations in the braid regions, approach, and wrap themselves around the primary K-H rolls, they generate streamwise vortices in the crossflow ($Y$, $Z$)-plane.

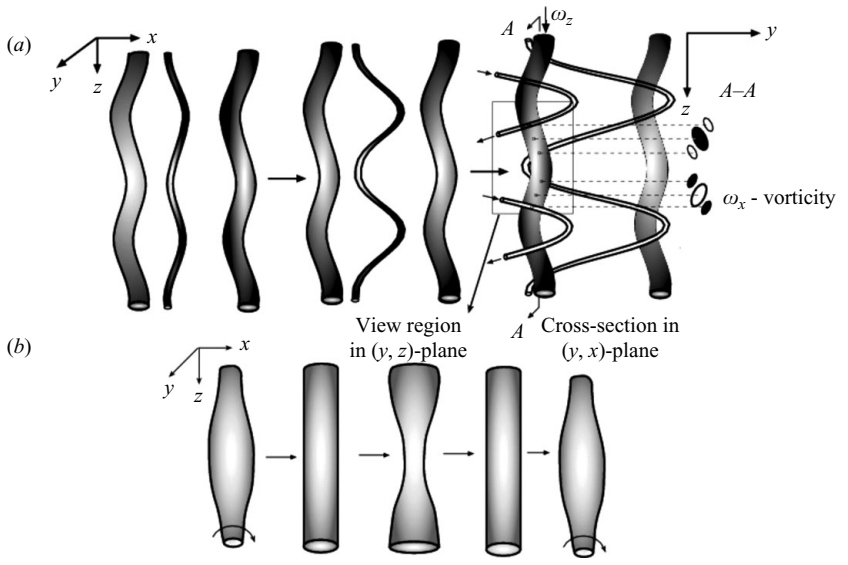


FIGURE 7. Sketch of spatial development of different three-dimensional disturbances: (*a*) translative instability (bending), (*b*) bulging.

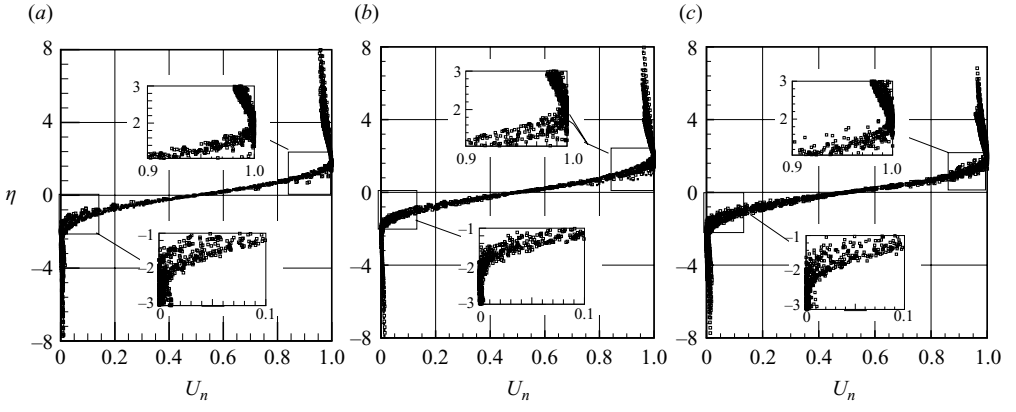


FIGURE 8. Normalized velocity profiles along the mixing layer measured by two cross-wire probes: $U_n = (U - U_{2min})/(U_{1max} - U_{2min})$. (*a*) Two-dimensional fliperon, $A = 1.5$ mm; (*b*) three-dimensional, 1.5 mm; (*c*) three-dimensional, 3 mm.

Three pairs of streamwise vortices appear in the cross-stream projection shown in figure 7: the central pair reflects the bending of the primary roll while two other pairs correspond to the rib vortices that are in the vicinity of the primary roll, one above and the other below it (figure 7*a*). These patterns were observed in the present experiment and in CFD computations of temporally developing mixing layer and they will be discussed later.

The approximate collapse of the normalized velocity profiles (figure 8) measured at various cross-sections beginning at $x = 100$ and ending at $x = 1000$ mm during periodic excitation, is a reasonable indicator that the local $\theta$ remains an appropriate parameter for normalization even in the case when the momentum thickness varies across the span. The velocity profile is not well represented by an 'error function'

or by a hyperbolic tangent function (tanh) as is often assumed in the literature (i.e. $(U-U_1)/(U_2-U_1)=\tanh\eta$; see Michalke 1965) because $(U-U_1)/(U_2-U_1)>1$ on the high-velocity side of the flow. The exact reason for this excess of velocity is not well understood, it may stem from the induction caused by the large spanwise rolls that transport high-velocity fluid toward the low-speed side, or by the limited size of the facility and the associated boundary-layer build-up on the solid walls.

The integration domain in the determination of $\theta$, had to be restricted to the location of this overshoot, as was also done by Gaster *et al.* (1985). Since the velocity profiles measured in the two-dimensional case encompass Regions I to III (figure 2), we expect to see a scatter, particularly near the outer boundaries of the mixing layer. The scatter exceeding experimental uncertainty is associated with the finite amplitude of the large spanwise vortices that are inclined differently in each of the regions observed. Such scatter indeed occurs (see the insets in figure 8) and it is most noticeable on the low-speed side of the flow whenever the plane K-H rolls are dominant. This occurs not only when the two-dimensional fliperon oscillates, but also when the chevron fliperon oscillates at the high amplitude of $A=3$ mm. When the chevron fliperon oscillates at the lower amplitude of 1.5 mm, the scatter on the low-velocity side is much smaller, but it is more noticeable on the high-velocity side. Flow visualization carried out by Nygaard & Glezer (1991) suggests that rib vortices are most noticeable on the high-velocity side of the K-H rolls because of the strain associated with the roll-up process at the end of the linear amplification cycle.

Measurements of $y_0$ and $\theta$ along the span were undertaken at various distances from the trailing edge of the splitter plate, but only the data at $x=420$ mm or $Rx/\lambda_x=1.03$ are presented in figure 9. The spanwise variations of both quantities downstream of the two-dimensional fliperon are very small at all distances from the splitter plate, proving the two-dimensionality of the mean flow. Forcing the chevron fliperon at $A=1.5$ mm results in slight undulations in $\theta$ along the span whose period corresponds to the spanwise wavelength of the chevron and its second harmonic. This stems from the thickening of the mixing layer opposite the cusp in the fliperon which imparts a higher amplitude of the oscillation onto the flow. Such undulations were also observed at closer distances to the fliperon. At $A=3$ mm, a strong magnification of $\theta$-undulations in the spanwise direction took place opposite the cusp that imparted the largest harmonic amplitude to the flow (with no second harmonic being present), indicating a strong amplification of the input perturbation that resulted in a local bulging of the primary spanwise rolls. This could also be inferred from figure 6(*c*).

The spanwise distribution of $y_0$ for the cross-section located 420 mm downstream from the partition is presented in figure 9(*b*). With the chevron fliperon oscillating at $A=1.5$ mm, $y_0$-undulations are observed in the spanwise direction distorting (bending) the location of the vortex cores. The spanwise period of these undulations corresponds to the spanwise wavelength of the chevron, suggesting that the fliperon's oscillations have little effect on the spanwise $y_0$-location. Thus the maximum $y_0$-displacement downwards occurs opposite the notch. For $A=3$ mm, the transverse undulations in $y_0$ are smaller owing to an obvious presence of a second harmonic in $\lambda_z$ that also displaces the mixing layer downward opposite a cusp. This indicates that the local input amplitude of the excitation affects $\theta$ by increasing the diameter and presumably the circulation of the large eddies, which resist better the bending that is imposed on these rolls by the shape of the jagged trailing edge of the partition. It is believed that the classical K-H rolls bend, bulge and perhaps merge under this type of excitation. Direct numerical simulations of temporally developing mixing layers (Rogers & Moser 1992; Schoppa *et al.* 1995), show that bending, and bulging of the primary rolls have

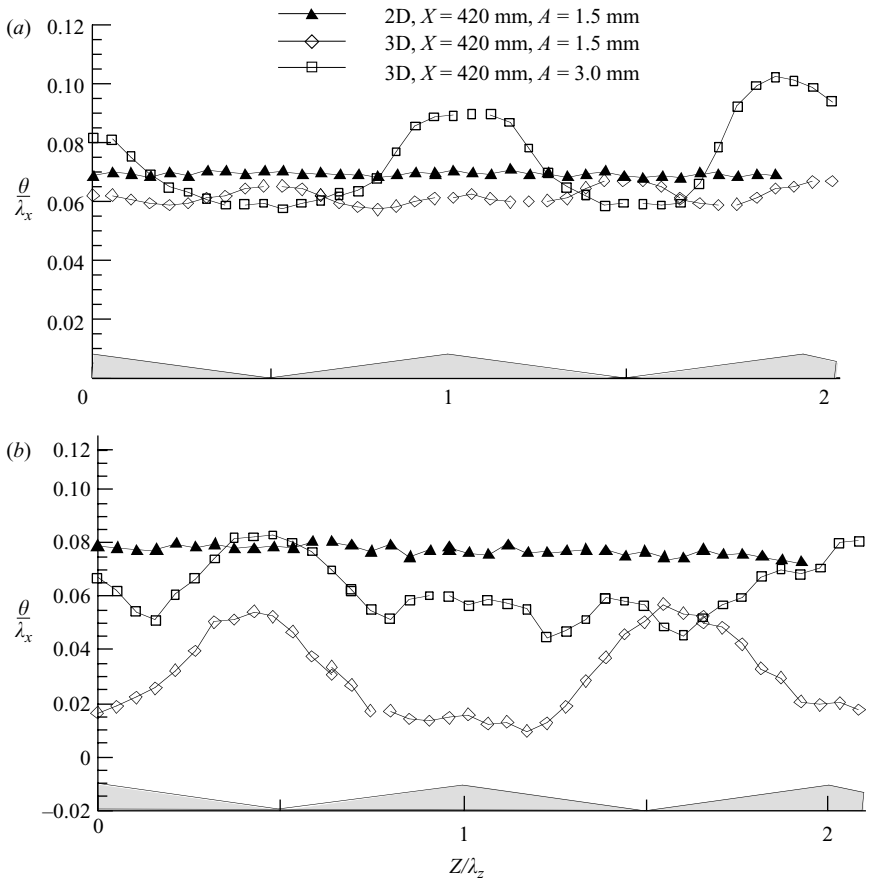


FIGURE 9. Spanwise distributions for various amplitudes of the fliperon at streamwise plane $Rx/\lambda_x = 1.03$ of: (*a*) normalized momentum thickness, (*b*) $(y_0/\lambda_x)$.

been caused by different initial perturbations that have been associated with different instability mechanisms.

### 3.2. *Coherent structures*

Although the lateral distributions of the $u_{coh}$ and $v_{coh}$ components of the velocity fluctuations in the two-dimensional forced mixing layer, are well known (Gaster *et al.* 1985), they were measured again and some of them presented for the sake of completeness. The amplitudes, phases and the cross-correlations of both components of velocity at the fundamental frequency, obtained by a Fourier transform of their coherent part after making a triple decomposition to mean, coherent and turbulent parts are shown in figure 10. The typical behaviour of the forced mixing layer is apparent. The coherent structures occupy the entire width of the mixing layer and they increase in size at the same rate as the mean flow (it should be remembered that the lateral coordinate on the figures is normalized by the local $\theta$ that increases in the direction of streaming). The phase distributions and Reynolds stress distributions are also typical of two-dimensionally forced mixing layers, indicating that kinetic energy is extracted from the mean flow to the coherent structures in Region I ($Rx/\lambda_x < 1.13$ or $x < 460$ mm), while the energy flows in the opposite direction in Region II (i.e. the coherent Reynolds stresses reverse their sign at $Rx/\lambda_x < 1.23$ as seen in figure 10*c*). As

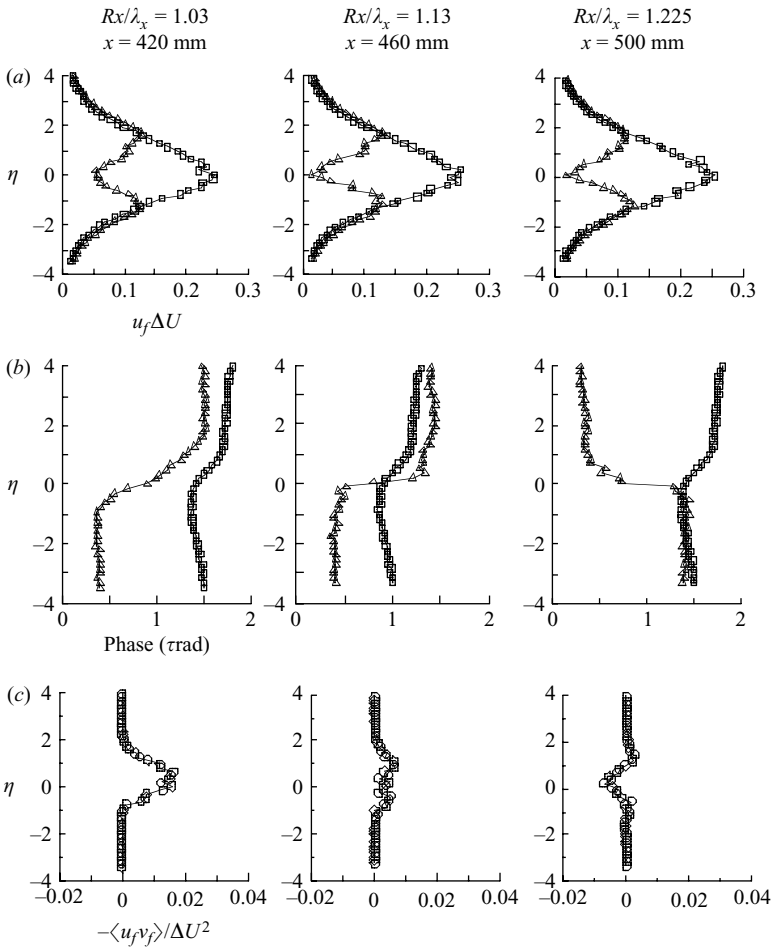


FIGURE 10. Crossflow distribution of total and random velocity fluctuations. Two-dimensional fliperon, $A = 1.5$ mm. □, $v_f$; △, $u_f$.

a consequence, the total coherent energy associated with the transverse fluctuations $\int \langle v_f \rangle \mathrm{d}y$ increased rapidly for $Rx/\lambda_x < 1.03$ while remaining almost constant in the range $1.03 < Rx/\lambda_x < 1.25$ and decaying thereafter.

Sample distributions of total intensities (obtained by double decomposition of the equations of motion) and their residual incoherent components (obtained by subtracting the coherent, phase-locked and ensemble-averaged values of these velocity fluctuations, from the total unsteady part of the motion) are compared in figure 11. The root-mean-square (RMS) values of the normal stresses shown are normalized by $\Delta U$. At very large distances ($x \approx 1000$ mm), the phase-locked coherent part of the motion forced at 20 HZ, is so small that the incoherent and the total intensities are equal, suggesting that the motion that has been imposed by the fliperon has dissipated. Most of the differences between random $v'$ and the total velocity fluctuations, which also include the coherent part, $v'_{total}$ in Region II ($Rx/\lambda_x > 1.13$) occur at the centre where $(v'_{total})_{max} \gg (v')_{max}$. At the beginning of Region I, $(v'_{total})_{max}$ is only slightly larger than $(v')_{max}$ because the amplitude of the coherent motion is still small, but it becomes large around $Rx/\lambda_x \approx 1$.

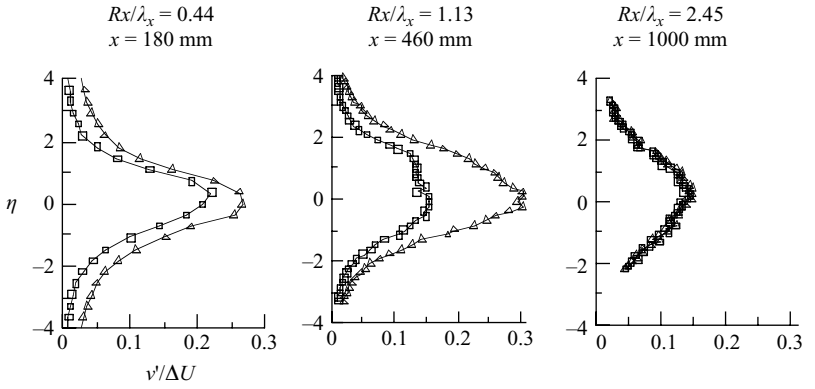


FIGURE 11. Lateral distribution of the coherent $\langle u_f \rangle$ and $\langle u_f v_f \rangle$ for the two-dimensionally perturbed mixing layer. $A = 1.5$ mm, $v$ random. □, $v'$; △, $v_{total}$.

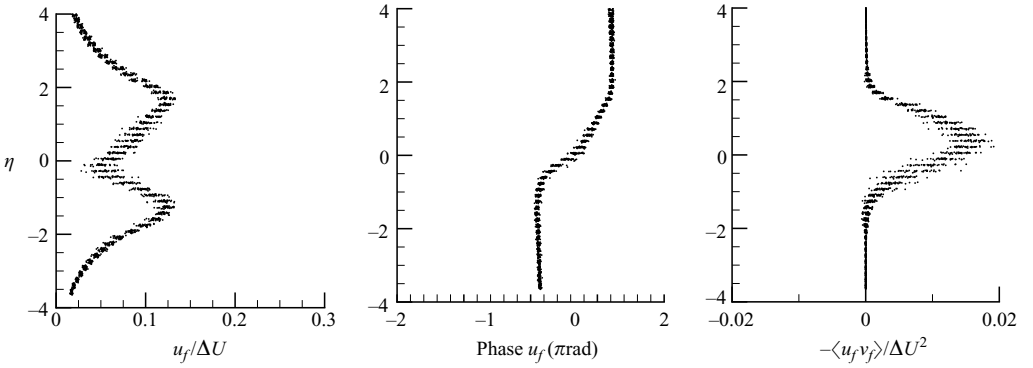


FIGURE 12. Lateral distribution of normalized streamwise velocity amplitudes, phases and $\langle u_f v_f \rangle$ correlations for the two-dimensionally perturbed mixing layer. $A = 1.5$ mm, $x = 420$ mm, $Rx/\lambda_x = 1.03$.

The spanwise variations of the lateral distributions of the fundamental velocity amplitudes $u_f$ and the point-correlations between different velocity components $\langle u_f v_f \rangle$ for the two-dimensional excited flow, were assessed at 40 spanwise locations (adjacent measurements were separated from one another by 4 mm) at various streamwise distances from the splitter plate. The distribution of the amplitude at the frequency of excitation, its phase, and the dimensionless coherent Reynolds stress indicate that the scatter among the 40 lateral distributions is small, but it increases slightly in the direction of streaming. An example of this two-dimensionality is shown in figure 12. The increase in the scatter along the span is associated with the direction in which energy is being transferred between the coherent structures and the mean flow. When the coherent structures are amplified, the scatter, even in the coherent Reynolds stress, is negligible. The spanwise scatter in the RMS of the incoherent (random) velocity fluctuations, determined through the triple decomposition procedure, is small everywhere (not shown).

Forcing the three-dimensional-fliperon at $A = 1.5$ mm results in a strong spanwise scatter of both amplitudes and phases of the fundamental fluctuations of velocity within the mixing layer. The lateral amplitude and phase distributions of the coherent velocity fluctuations opposite a notch and a cusp are shown as solid and dashed lines

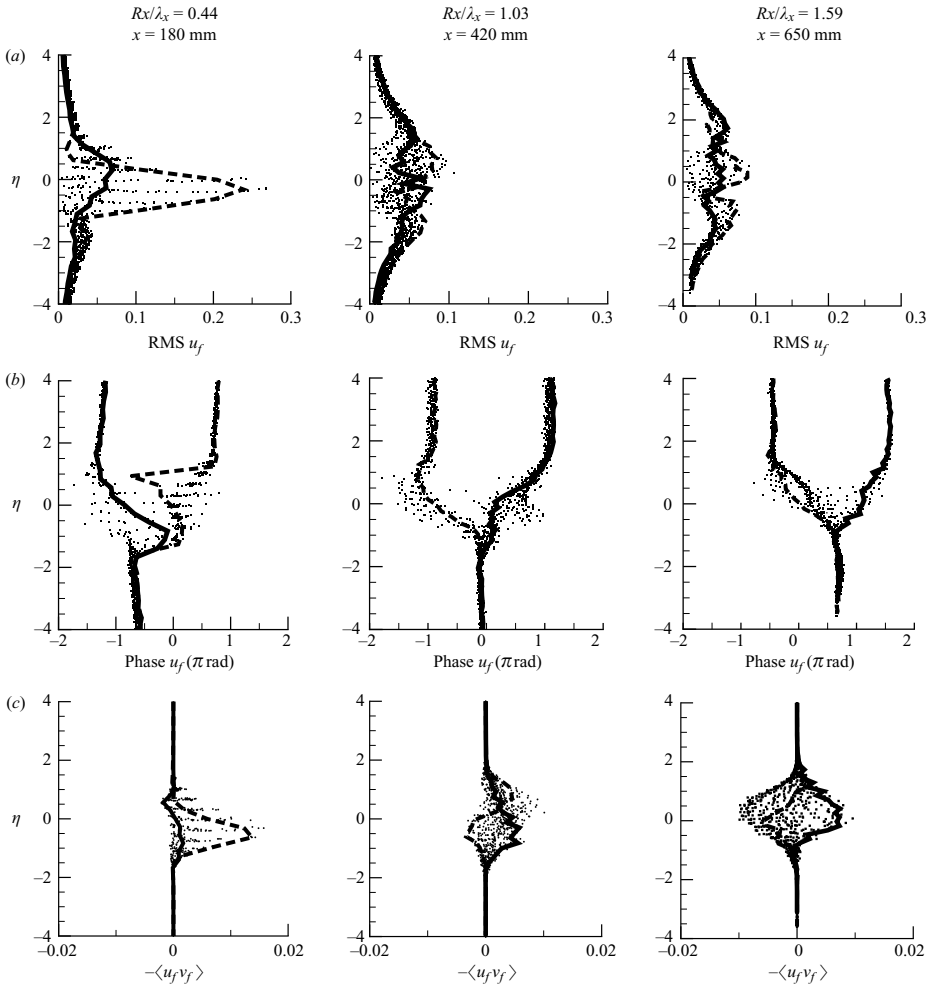


FIGURE 13. Lateral distribution of coherent velocities, phases and normalized velocity correlations at three streamwise cross-sections and numerous spanwise ones for the three-dimensionally perturbed mixing layer. Solid line, the movable probe opposite the notch; dashed line, opposite the cusp. $A = 1.5$ mm.

in figure 13, respectively. Also, the lateral distributions presented in this figure use the normalized transverse coordinate $\eta$, in which the average location of the centre of the mixing layer, $y_0$, was subtracted. Consequently, the average transverse bending of the large eddies was eliminated from this figure, allowing us to concentrate more on the streamwise displacement of the large eddies along the span. This displacement is periodic owing to the up and down movement of the jagged trailing edge of the splitter plate.

In the potential flow, away from the mixing layer, both amplitudes and phases measured opposite the cusp and the notch coincide (when $2\pi$ is added to the data on the high-speed side). However, within the core of the mixing layer, there are large differences in the coherent intensities and their phase distributions. Most importantly, the phase distributions congregate around two extremes that are barely affected by increasing the distance from the fliperon: one extreme corresponding to the location

opposite a cusp and the other opposite the notch (trough). In two-dimensional flow, one of the extremes would have represented an amplifying disturbance and the other a decaying one. This phase distribution is related to the inclination of the large K-H rolls relative to the mean flow field. Whenever the large axis of these elliptical eddies is almost orthogonal to the tangent of the velocity profile at the highest mean velocity gradient, these eddies amplify, but when the inclination of these eddies coincides with the inclination of this tangent, they decay. The relation between inclinations of the large eddies and the sign of the Reynolds stress was observed by Browand & Ho (1983) and more recently derived theoretically by Smyth & Peltier (1989). The first roll-up resulting from a K-H instability is expected to be parallel to the trailing edge, provided that this instability is the dominant one (Kibens *et al.* 1986), therefore first rolls generated downstream of the opposing parts of the 'chevron' trailing edge are expected to be inclined in the $(x, z)$-plane at opposite angles to the flow direction. Provided these rolls are approximately circular to begin with, (measurements in the plane mixing layer indicate that they are circular before they start decaying farther downstream, Zhou & Wygnanski 2001), their cross-sections in the $(x, y)$-plane will be elliptical with their large axis being inclined either backward or forward relative to the high-speed stream. Consequently, the inclination of eddies in the $(x, z)$-plane contributes to their local amplification or decay along the span and therefore results in a large spanwise variation in intensities. Indeed, the $u_f$ fluctuations, change their amplitude (figure 13*a*) and their phase (figure 13*b*) depending on the $z$ location of the probe relative to the chevron and thus resemble either amplifying or decaying K-H modes. The spanwise inclination of the large eddies has a major effect on the coherent Reynolds stresses which are negative initially (at $Rx/\lambda_x = 0.44$) downstream of a cusp ($\langle u_f v_f \rangle)_{max} \approx 0.013$ while being negligible downstream of a notch. At larger distances (e.g. $Rx/\lambda_x > 1$) both positive and negative coherent Reynolds stresses are observed, depending on the precise spanwise position of the probe (figure 13*c*). Positive $\langle u_f v_f \rangle_{max}$ occur downstream of a cusp on the low-velocity side of the flow ($\eta < 0$), because it is associated with a roll-up that is triggered earlier by higher amplitudes of the coherent K-H instabilities. Up to $Rx/\lambda_x = 1$, the mean rate of divergence of this mixing layer was uniform across the span (figure 6*c*), but downstream of this location the rate of divergence opposite the cusp decreased, presumably because the amplitude of the coherent motion at this spanwise location was higher and it saturated. At $Rx/\lambda_x = 1.6$, the coherent Reynolds stresses corresponding to the intermediate spanwise locations between a notch and a cusp, are frequently more negative than at both of these spanwise extremes.

The lateral distributions of turbulent intensity and Reynolds stress that were obtained by triple decomposition of the time-dependent signal, spread out across the mixing layer with increasing $x$, as they did when the two-dimensional fliperon was used (only the Reynolds stresses are plotted in figure 14). However, this spreading rate is associated with the random Reynolds stresses, not the coherent ones as happened with the two-dimensional fliperon. We may compare the correlation of the random components $\langle u'v' \rangle_{max}$ measured at $Rx/\lambda_x \geqslant 1.03$ for the two fliperons used and note how much larger this quantity is for the chevron fliperon. The turbulent quantities are fairly uniform across the span and suggest continuous transfer of kinetic energy from the mean motion to the random fluctuations.

Simultaneous measurements using two cross-wire probes, with one of the probes being stationary at a fixed spanwise location while the other traverses along the span, enabled the computation of spatial correlations between these probes. The closest separation distance between the probes was 4 mm, it was also the step size by which $\Delta z$ was increased. The maximum separation distance between the probes was 160 mm,

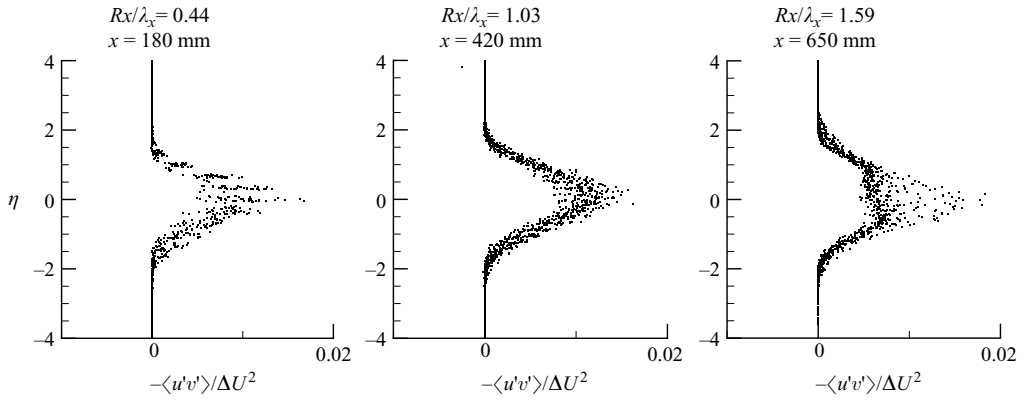


FIGURE 14. Lateral distribution of Reynolds stress for the three-dimensionally perturbed mixing layer. $A = 1.5$ mm.

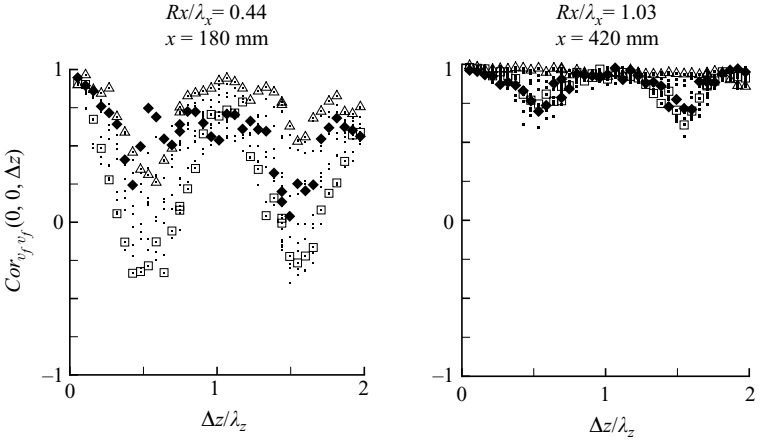


FIGURE 15. Spanwise correlations of fundamental normal velocity component in three-dimensionally flow perturbed. The entire range in the normal direction is $y = \pm 20$ mm; △, $y = +20$ mm; ◆, $y = -20$ mm; □, $y = 0$. $A = 1.5$ mm.

and it comprised more than 2 wavelengths of the chevron. The spanwise two-point correlations representing the coherent portion of the normal velocity fluctuations are approximately equal to unity [$Cor_{v_f v_f}(0, 0, \Delta z) \approx 1$] at larger distances from the two-dimensional fliperon. This correlation is somewhat lower at small distances downstream of the fliperon in the core of the mixing layer, presumably because of the remnants of the turbulence shed from the splitter plate. The correlation measurements were carried out at 11 lateral locations, spanning 40 mm above and below the plane that constitutes the continuation of the splitter plate.

Strong bending and/or bulging of the primary rolls in the experiments using a three-dimensional fliperon lead to large initial variations of $Cor_{v_f v_f}(0, 0, \Delta z)$ as a function of the spanwise distance. The results presented in figure 15 are for $A = 1.5$ mm, but similar results were observed at the higher amplitude of $A = 3$ mm. Since these measurements were carried out at a constant $y$ location, the clearly visible footprints of the cusps and notches of the fliperon may be due to bending of the large coherent structures generated in their wake. A negative correlation is seen at $\Delta z/\lambda_z = 0.5$

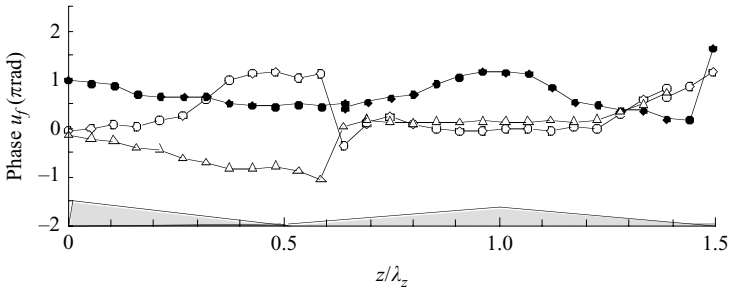


FIGURE 16. Phase distribution of streamwise coherent velocity component along the span at three streamwise planes: ○, $Rx/\lambda_x = 0.44$, $x = 180$ mm; ●, $Rx/\lambda_x = 1.03$, $x = 420$ mm; △, $Rx/\lambda_x = 1.59$, $x = 650$ mm. $A = 1.5$ mm. $y = 0$.

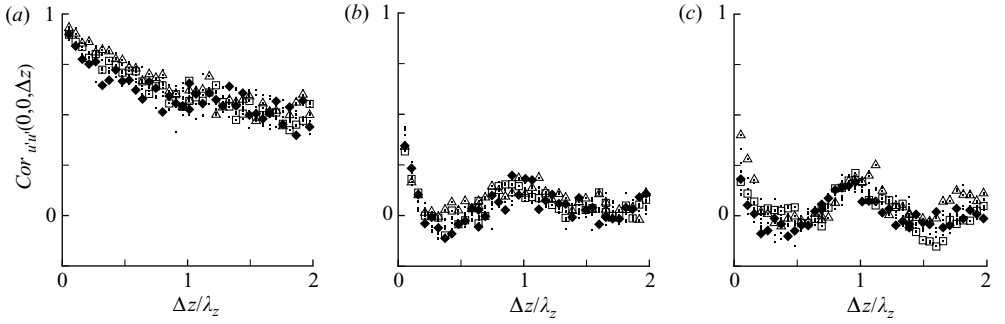


FIGURE 17. Spanwise correlations of random streamwise velocity component in two- and three-dimensionally flow perturbed. The entire range in normal direction is $y = \pm 20$ mm, Δ, $y = +20$ mm, ◆, $y = -20$ mm, □, $y = 0$. $Rx/\lambda_x = 1.03$, $x = 420$ mm. (*a*) Two-dimensional, $A = 1.5$ mm; (*b*) three-dimensional, 1.5 mm; (*c*) three-dimensional, $A = 3$ mm.

at $y = 0$ and $Rx/\lambda_x = 0.44$ whereas at $y = \pm 20$ mm, $Cor_{v_f v_f}(0, 0, \Delta z) \approx 0.25$ before returning to approximately unity at $\Delta z/\lambda_z = 1$. At $y = \pm 20$ mm, the minimum of $Cor_{v_f v_f}(0, 0, \Delta z) > 0$. At $Rx/\lambda_x = 1.03$, the minimum of $Cor_{v_f v_f}(0, 0, \Delta z) \approx 0.6$ corresponding to $y = 0$ and $y = -20$ mm while it maintained its two-dimensional value of $Cor_{v_f v_f}(0, 0, \Delta z) \approx 1$ on the high-velocity side of the flow.

The spanwise phase shifts of $u_f$ collected at $y = 0$ plotted in figure 16, are large in the centre of the flow and on its low-velocity side while being negligible on the high-velocity side of the flow. A phase shift of $\pi$ occurred opposite a notch located at $z/\lambda_z = 0.5$ at two distances from the fliperon, $x = 180$ and 650 mm corresponding to $Rx/\lambda_x = 0.44$ and 1.59. It suggests that the hot-wire probe crossed the centre of the large eddy at that location, implying that the eddy is bent. The amplitude of the bending varies in a periodic fashion in the direction of streaming, because the distance between the two measurement locations corresponds approximately to $Rx/\lambda_x \approx 1$, while half-way between these measurement locations (i.e. at $Rx/\lambda_x = 1.03$), gradual small phase shifts were observed.

The correlation of the random component $u'$, $Cor_{u'u'}(0, 0, \Delta z)$, diminished with increasing separation distance, $\Delta z$, between the probes, but it remained exceptionally high when the two-dimensional fliperon was used. This even held in the very interior of the mixing layer, at $y = 0$, suggesting that the random oscillations are contained within the large and regular K-H rolls (figure 17). For example at $Rx/\lambda_x = 1.03$, the minimum correlation coefficient of the random component was $Cor_{u'u'}(0, 0, \Delta z) \approx 0.5$

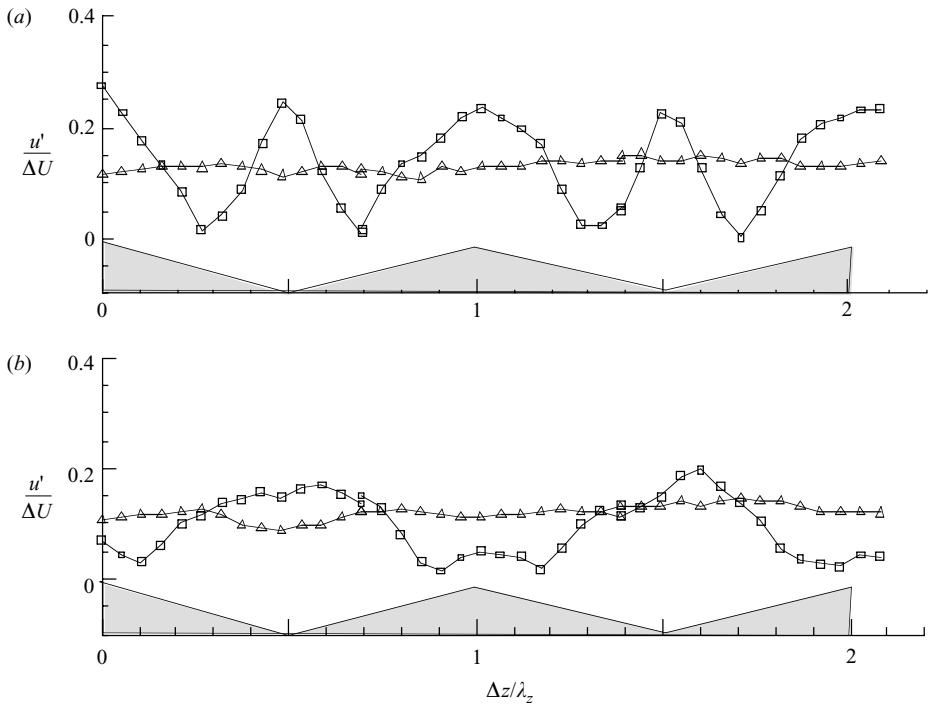


FIGURE 18. Coherent □, and random △, spanwise distributions of intensities of streamwise velocity component measured in streamwise plane coinciding with partition plane, $y = 0$, at two streamwise locations. Three-dimensional fliperon, $A = 3$ mm. (*a*) $x = 180$ mm, $Rx/\lambda_x = 0.44$; (*b*) $x = 420$ mm, 1.03.

and it decreased slightly with increasing distance from the trailing edge of the fliperon (only the data collected at $Rx/\lambda_x = 1.03$ is shown). The same correlation coefficient decreased rapidly downstream of the chevron fliperon oscillating at $A = 1.5$ mm. Remnants of the spanwise wavelength of the chevron are detectable, generating a slightly negative correlation around $\Delta z/\lambda_z \approx 0.5$ and 1.5 (figure 17). The footprint of the chevron fliperon has a stronger presence when the fliperon's amplitude was increased to $A = 3$ mm. It seems that higher-amplitude oscillations that vary along the span due to the chevron's shape result in locally thicker K-H rolls modulating the random motion in the mixing layer downstream.

For better understanding of the interaction between the coherent and random eddies in the perturbed three-dimensional-mixing layer, the variations in the intensity of both components along the span are discussed. The spanwise distributions of streamwise intensities $u'/\Delta U$ are presented in figure 18 for the 3 mm chevron fliperon oscillations. Coherent and random velocity fluctuations measured directly downstream of the splitter plate's trailing edge, are used for comparison. The results are somewhat surprising because only at shorter distances, $Rx/\lambda_x \leqslant 0.44$, are strong periodic variations of streamwise coherent intensities observed. Comparing the data obtained at $Rx/\lambda_x = 0.44$ with that at $Rx/\lambda_x = 1.03$, we can see the decay of the coherent motion. At shorter distances, high-intensity coherent oscillations occur both opposite a cusp and a trough in the chevron fliperon, doubling the spanwise wavenumber of these intensity concentrations. Bending of the vortices in the trough region is mostly responsible for the enhanced intensity of the coherent motion there,

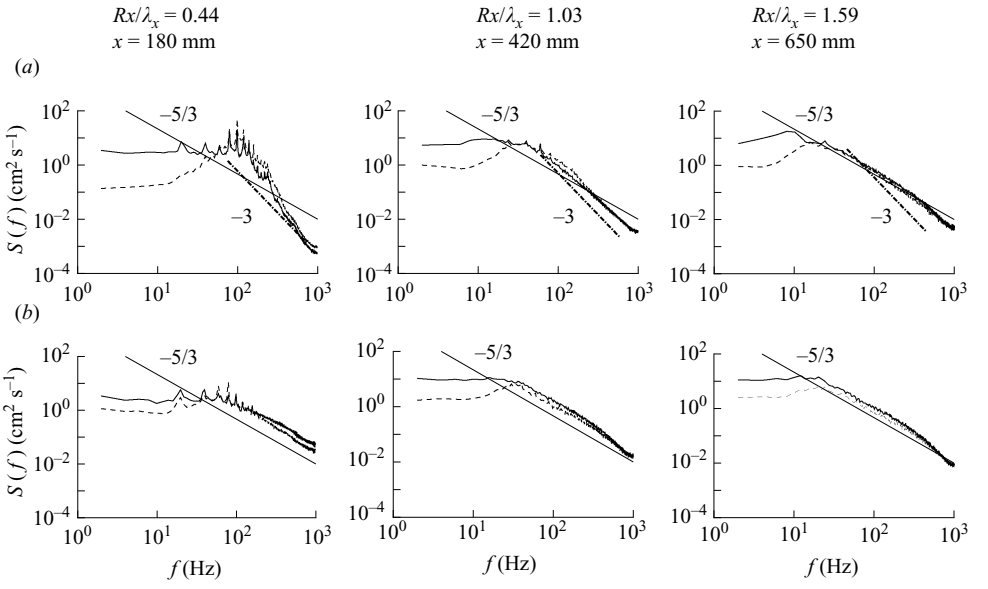


FIGURE 19. Energy spectra for both non-coherent velocity components measured in (*a*) two- and (*b*) three-dimensional-perturbed mixing layer at $y = 0$: solid line-streamwise velocity component; dashed line, normal velocity component. $A = 1.5$ mm.

while the larger amplitude imparted by the chevron fliperon in the cusp region is still visible at $Rx/\lambda_x = 1.03$. The random fluctuations are evenly distributed along the span of the mixing layer regardless of the type of the initial perturbations imposed on the flow (figure 18).

### 3.3. *Energy spectra*

Spectral densities of velocities $u'$ and $v'$ measured at $y = 0$ are presented in figure 19 where the streamwise component of the turbulence intensity is shown as a solid line. The results were obtained by averaging over 400 records in order to reduce the noise. The results corresponding to the two-dimensional oscillating fliperon tests show that the power spectrum approaches Kolmogorov's $-5/3$ slope at large distances from the fliperon, in what might be expected to be the inertial subrange. Spectral densities of velocity fluctuations computed when a three-dimensional fliperon was installed and was oscillating at the lower amplitude $A = 1.5$ mm, possess this slope at $Rx/\lambda_x = 0.44$ from the partition suggesting that in this case the flow within the spanwise rolls is fully turbulent much closer to the trailing-edge splitter plate. Thus, the mixing transition might have occurred much earlier in the three-dimensional than in the two-dimensional case.

The large correlation coefficient of the random velocity fluctuations measured downstream of the two-dimensional fliperon (figure 17), indicates that the incoherent fluctuations in the core of the large rolls are a mixture of two-dimensional and three-dimensional turbulence, which becomes mostly three-dimensional at larger distances from the fliperon. To stress this observation, a straight line having a slope of $-3$ is also drawn in figure 19(*a*). This line represents a typical slope associated with two-dimensional turbulence (e.g. Kit & Tsinober 1971). The agreement of this slope with the data at $x = 420$ mm is startling. The main difference between the two-dimensional coherent and random structures is related to their phase which is determinate in the first case and random in the second. If the turbulence had been purely

two-dimensional, the spanwise correlation should have been unity. However, because it is a mixture of two- and three-dimensional turbulence, the three-dimensional effects dominate at large distances from the fliperon (figure 19).

In the low-frequency range, ($f < 50$ Hz) the normal velocity fluctuations, $v'$, are always smaller than the $u'$. This is particularly obvious in the two-dimensional case where $v'$ was an order of magnitude lower in this case (figure 19).

### 3.4. *SPIV measurements of structures*

The mapping of three-dimensional coherent structures by using hot-wire anemometry is a difficult task that can be much better performed using SPIV. In spite of its poor temporal resolution, it has the ability to discover spatial coherent structures, particularly streamwise ones that have to be mapped in the cross-flow plane. Phase-locked and random phase measurements of velocity and vorticity were carried out in two planes, streamwise ($(x, y)$-plane) and spanwise ($(z, y)$-plane), in order to study the primary two-dimensional and the secondary three-dimensional coherent structures.

Streamwise vorticity plots measured in the $(y, z)$-plane at distances of 200 and 400 mm from the trailing edge of the weakly excited jagged splitter plate (i.e. oscillating chevron fliperon) are shown in figure 20. These plots reveal the spanwise periodicity of the streamwise vortices induced by the jagged trailing edge. The spanwise period $\Delta z/\lambda_z = 1$ corresponds to the wavelength of the three-dimensional-fliperon, but the intensity of the vorticity observed depends on the phase and the distance at which the data were acquired, suggesting a correlation between streamwise and spanwise vorticity concentrations. At $x = 200$ mm and at a phase angle of 270° relative to the forcing signal applied to the fliperon (figure 20*a*), three concentrations of alternating sign of vorticity are visible to the left and to the right of each cusp. The sign of vorticity changes across the $(x, y)$-plane which passes through the cusp. The upper and the lower vortices represent the signature of rib vortices arriving from different braid regions in the $(y, z)$-plane as appear in the sketch (figure 7). The central vortex develops in the core of the primary roll and has a vorticity of a different sign from other vortices, as follows from the sketch. The sign of a set of vortices originating from each side of the cusp is alternating as predicted by figure 7. The $y$-locations of the vortex cores are approximately $y/\lambda_z = -0.22$, $-0.05$ and 0.1 from $y = 0$ and they move slightly away from the cusp as $y$ is increased. If the phase-locked ensemble-averaged map was taken when a core of the spanwise roll was bisected by the light sheet, the alternating sign of vorticity in the $y$-direction may stem from the streamwise vortex being rolled around the primary transverse K-H roll. The schematic diagram shown in figures 7 explores this scenario. It shows how a spanwise vortex that is bent along the span is being strained and rolled around neighbouring spanwise vortices that managed to retain their predominantly spanwise vorticity. In this manner, the spanwise vorticity of the stretched vortex is converted into streamwise vorticity with discrete concentrations that are similar to those measured in figure 20(*a*) at the phase angle of 270°. This plot has been expanded and presented in figure 21(*a*) because, as mentioned above, it provides a qualitative agreement with time-resolved Navier–Stokes computations (Kit, Gelfgat & Nikitin 2007) in a temporally developing mixing layer that revealed similar structures in the spanwise flow plane (figure 21*b*). There is therefore little doubt that the bending of the spanwise rolls creates strong streamwise vortices which were detected in this investigation and which affect the level of turbulence in the mixing layer.

We can postulate that the jagged trailing edge triggers the translative instability in the core of the primary spanwise vortex (Rogers & Moser 1992) and the observations

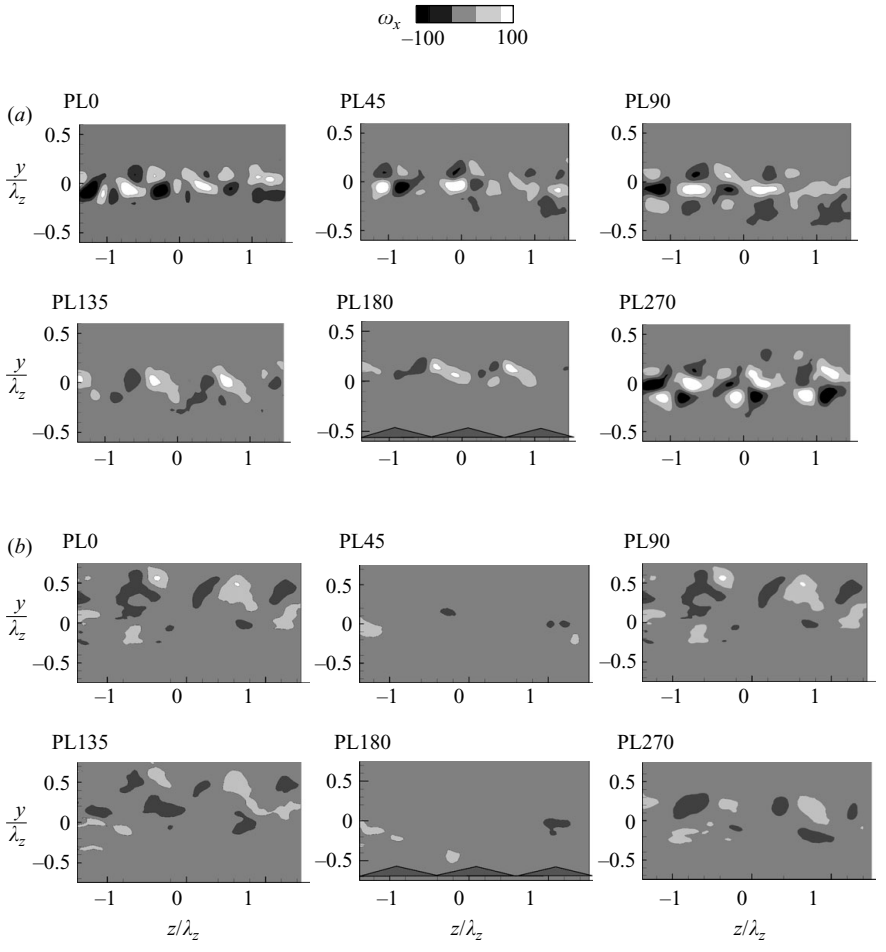


FIGURE 20. Spanwise distribution of phase-locked streamwise vorticity contours obtained by applying SPIV at six initial phases measured at two streamwise locations: (*a*) $Rx/\lambda_x = 0.49$, (*b*) $Rx/\lambda_x = 0.98$. The lateral coordinate of the SPIV patterns is rendered dimensionally using $y/\lambda_z$. Three-dimensional fliperon, $A = 1.5$ mm. (*a*) $x = 200$ mm, (*b*) $x = 400$ mm.

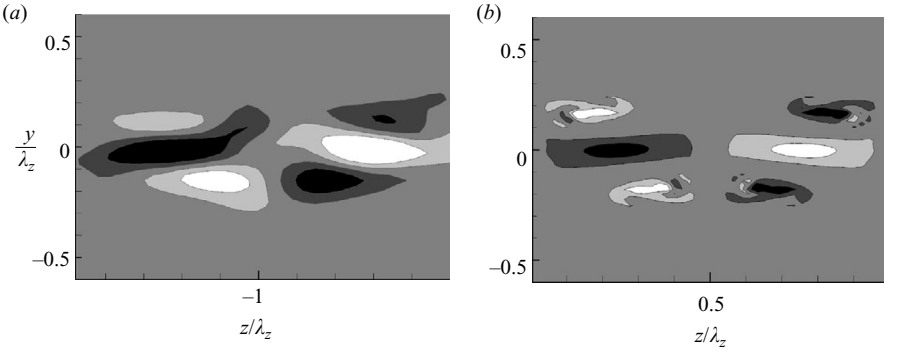


FIGURE 21. Qualitative comparison of streamwise vorticity contours in spanwise plane crossing the primary roll: (*a*) experiments, (*b*) temporal three-dimensional computations.

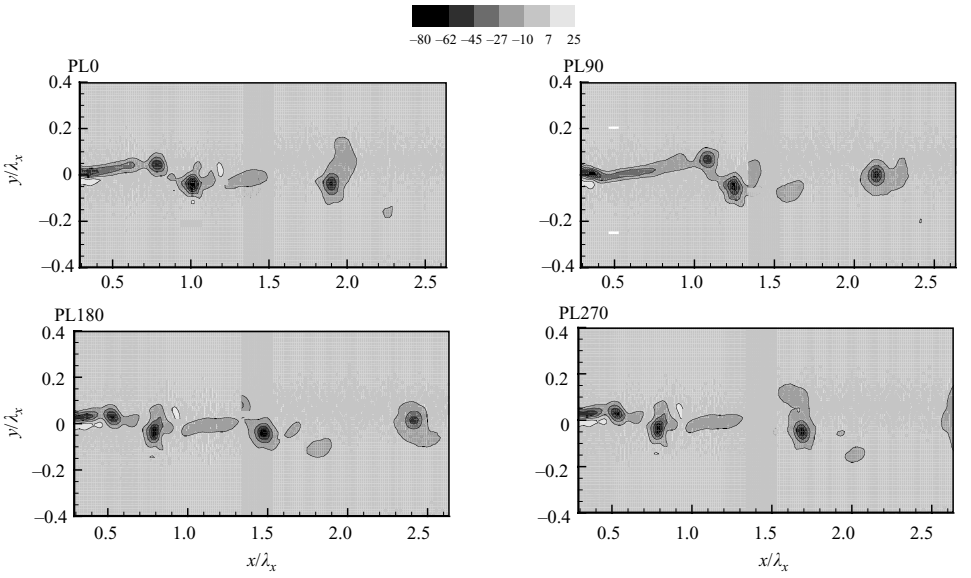


FIGURE 22. Streamwise distribution of spanwise vorticity contours comprised from mean and phase-locked data measured at four phases relative to the forcing in the plane of symmetry, $z = 0$, $f_e = 20\,\mathrm{Hz}$, $\lambda_x = 175\,\mathrm{mm}$. $A = 1.5\,\mathrm{mm}$.

reflect upon the rib vortices winding over the primary spanwise vortex. At other phase delays (figure 20*a*), the light sheet illuminates the rib vortices at different positions relative to the core or the braid and this may change the number of vortices being observed. For example at a phase of 180° and $Rx/\lambda_x = 0.49$, only one array of counter-rotating vortices whose cores are centred around $y/\lambda_z = 0.15$ can be seen. It has been suggested that at this cross-section, which is close to the fliperon ($x/\lambda_x \sim 1$), the second harmonics are strong, resulting from the nonlinear generation of perturbations by the fliperon and its significant amplification in the region where the thickness of the mixing layer is small. Thus the actual structure of the primary vortices is determined by the two frequencies, the fundamental excitation frequency and its second harmonic. An additional confirmation of this effect can be deduced from the measurements made in the $(x, y)$-plane (see figure 22). It can be readily seen that at larger distances ($x/\lambda_x > 1$), the primary vortices are separated by a distance corresponding to the fundamental wavelength, $\lambda_x$; however, close to the splitter plate, the vortex spacing is approximately $\lambda_x/2$. This may explain why at phase angle of 90° (that is 180°–$\lambda_x/2$–from 270°) in figure 20(*a*), three couples of vortex structures reappear. In the absence of the harmonic frequency, the light sheet would have illuminated the braid region at this phase and would have shown only two counter-rotating rib vortices. The appearance of one couple of counter-rotating vortices at phase of 180° also reinforces the above statement since the light sheet probably intercepts the braid region at this phase.

The intensities of phase-locked streamwise vortices decrease and their spanwise periodicity becomes less orderly when the distance of the measurement from the splitter plate was increased to $Rx/\lambda_x = 0.98$ or $x = 400\,\mathrm{mm}$ (figure 20*b*). It could be attributed to the strong interaction of both kinds of coherent vortices: primary spanwise rolls and secondary rib vortices, which lead to generation of smaller three-dimensional structures that eventually lead to turbulence. This interaction results in

suppression of secondary rib vortices. The hot-wire measurements confirm this trend. Similar results have been obtained at the higher amplitude of the fliperon oscillations of 3 mm. When a two-dimensional fliperon was used, the streamwise vortices were weak and randomly distributed in the crossflow plane. No natural periodicity along the span was observed.

The spanwise vorticity contours measured downstream of an oscillating chevron fliperon at four phases relative to the fliperon's forcing signal (figure 22) are reminiscent of but somewhat different from similar contours obtained in a two-dimensional forced mixing layer (e.g. Weisbrott & Wygnanski 1988). The first roll-up occurs closer to the fliperon, (at $Rx/\lambda_x = 0.35$) and it is immediately followed by another vortex that is displaced in the positive $y$-direction. The two vortices on either side of $Rx/\lambda_x = 0.4$ might represent a cross-section in a braiding process. The vortex observed around $Rx/\lambda_x = 0.8$ is stretched in the $y$-direction and disconnected from the other vortices in the array since the roll-up process depletes the braid region from spanwise vorticity.

## 4. Concluding remarks

A static chevron fliperon enhances a translative instability that bends the large spanwise Kelvin–Helmholz vortices and develops streamwise rib vortices. Three-dimensional harmonic perturbations, generated by an oscillating chevron fliperon, enhance the convective (K-H) instability and modulate the ensuing eddies along the span. Both effects create coherent streamwise vorticity near the partition's trailing edge, which lead to the development of streamwise vortex tubes (rib vortices and bent or bulging spanwise vortices) farther downstream. Two types of three-dimensional distortions of the primary spanwise rolls were observed: bulging and bending, where the latter takes place in both vertical ($y$ displacement at a given time) and streamwise directions detected by the variation in phase shift along the span. The integral characteristics of the mean flow, $\theta$ (the momentum thickness) and $y_0$ (the location of the centre of the mean velocity profile) attest to the type of the prevailing vertical distortion whereas the phase shift in the coherent motion attests to the streamwise bending. The streamwise vortices become less coherent with increasing distance from the fliperon. They seem to disappear in the straining field existing between adjacent K-H rolls and they are less regular and weaker within the rolls themselves. This might be an outcome of a strong interaction between the spanwise K-H type of rolls and streamwise vortex tubes.

Although the data presented corresponded to a single excitation frequency of 20 Hz, a considerable amount of data was also acquired at a frequency of 40 Hz. Since these experiments did not reveal any different qualitative results it was decided not to present them here.

Two-dimensional periodic excitation delays the development of three-dimensional turbulence. Incoherent disturbances derived from measurements by using triple decomposition, are strongly correlated in the spanwise direction, suggesting that they are either contained within predominantly two-dimensional structures or they are in fact two-dimensional. This is particularly true in Region I (figure 2). Only in Region III does this correlation decrease substantially. Examination of the power spectra lead to similar conclusions. While three-dimensional excitation by a chevron-shaped trailing edge results in $-5/3$ slope of the spectrum in the inertial subrange, two-dimensional excitation generates a slope of $-3$ over similar distances from the origin of the flow. This is typical of two-dimensional turbulence, whereas the

generation of Kolmogorov's $-5/3$ slope occurs much farther downstream, where internal instabilities generate three-dimensional turbulence.

The three-dimensional turbulence generated by a chevron splitter plate whether active or passive should be investigated more thoroughly in the future, because it may lead to quieter jet designs and to more efficient mixing processes, thus having a broad engineering implication.

This work is supported by the Israel Science Foundation (Grant 240/01), by the Bi-National Science Foundation (Grant 2004087) and in part by German-Israeli Foundation (Grant 794-145.10/2003-I).

## REFERENCES

Bernal, L. P. & Roshko, A. 1986 Streamwise vortex structure in plane mixing layers. *J. Fluid Mech.* **170**, 499–525.

Browand, F. K. & Ho, C. M. 1983 The mixing layer: an example of quasi two-dimensional turbulence. *J. Méc.* Special vol. 99.

Browand, F. K. & Latigo, B. O. 1979 Growth of the two-dimensional mixing layer from a turbulent and nonturbulent boundary layer. *Phys. Fluids* **22**, 1011–1019.

Browand, F. K. & Troutt, T. R. 1980 A note on spanwise structure in the two-dimensional mixing layer. *J. Fluid Mech.* **117**, 771–781.

Bell, J. H. & Mehta, R. D. 1992 Measurements of the streamwise vortical structures in a plane mixing layer. *J. Fluid Mech.* **239**, 213–248.

Buell, J. C. & Mansour, N. N. 1989 Asymmetric effects in three-dimensional spatially-developing mixing layers. *Seventh Symp. on Turbulent Shear Flows, Stanford University, August 21–23, 1989,* pp. 9.2.1–9.2.6.

Cohen, J. & Wygnanski, I. 1987 The evolution of instabilities in the axisymmetric jet. Part 1. The linear growth of disturbances near the nozzle. *J. Fluid Mech.* **176**, 191–219.

Craik, A. D. D. 1971 Nonlinear resonant instability in boundary layers. *J. Fluid Mech.* **50**, 393–413.

Gaster, M., Kit, E. & Wygnanski, I. 1985 Large-scale structures in a forced turbulent mixing layer. *J. Fluid Mech.* **150**, 23–39.

Gelfgat, A. & Kit, E. 2006 Spatial versus temporal instabilities in a parametrically forced stratified mixing layer. *J. Fluid Mech.* **552**, 189–227.

Ho, C. & Huerre, P. 1984 Perturbed free shear layer. *Annu. Rev. Fluid Mech.* **16**, 365–424.

Huang, L.-S. & Ho, C.-M. 1990 Small-scale transition in a plane mixing layer. *J. Fluid Mech.* **210**, 475–500.

Hussain, A. K. M. F. 1983 Coherent structures-reality and myth. *Phys. Fluids* **26** 2816–2850.

Konrad, J. 1976 An experimental investigation of mixing in two-dimensional turbulent shear flows with applications to diffusion-limited chemical reactions. PhD thesis, California Institute of Technology.

Kibens, V., Wlezien, R. W., Roos, F. W. & Kegelman, J. T. 1986 Trailing edge sweep and three dimensional vortex interactions in jets and mixing layers. *AGARD CP* 486.

Kit, E., Gelfgat, A. & Nikitin, N. V. 2007 three-dimensional simulation of secondary instability modes of KH billows in plane mixing layer. In preparation.

Kit, L. G. & Tsinober, A. B. 1971 On the possibility of realization and investigation of two-dimensional turbulence in a strong magnetic field, *Magnetohydrodynamics* **3**, 27–34.

Lasheras, J. C. & Choi, H. 1988 Three-dimensional instability of a plane free shear layer: an experimental study of the formation and evolution of streamwise vortices. *J. Fluid Mech.* **189**, 53–86.

Leboeuf, R. L. & Mehta, R. D. 1996 Vortical structure morphology in the initial region of a forced mixing layer: roll-up and pairing. *J. Fluid Mech.* **315**, 175–221.

Lin, S. J. & Corcos, G. M. 1984 The mixing layer: deterministic models of a turbulent flow. Part 3. The effect of plane strain on the dynamics of streamwise vortices. *J. Fluid Mech.* **141**, 139–178.

Marasli, B., Champagne, F. H. & Wygnanski, I. 1991 On linear evolution of unstable disturbances in a plane turbulent wake. *Phys. Fluids* A **3**, 665–674.

Metcalfe, R. W., Orszag, S. A., Brachet, M. E., Menon, S. & Riley, J. J. 1987 Secondary instability of a temporally growing mixing layer. *J. Fluid Mech.* **184**, 207–243.

Michalke, A. 1965 On spatially growing disturbances in an inviscid shear layer. *J. Fluid Mech.* **23**, 521–544.

Nygaard, K. J. & Glezer, A. 1990 Core instability of the spanwise vortices in a plane mixing layer. *Phys. Fluids* A **2**(3), 461–464.

Nygaard, K. J. & Glezer, A. 1991 Evolution of streamwise vortices and generation of small-scale motion in a plane mixing layer. *J. Fluid Mech.* **231**, 257–301.

Oster, D. & Wygnanski, I. 1982 The forced mixing layer between parallel streams. *J. Fluid Mech.* **123**, 91–130.

Oster, D., Wygnanski, I., Dziomba, B. & Fiedler, H. 1978 *The Effects of Initial Conditions on the Two-Dimensional Mixing Layer*. In Lecture Notes in Physics vol. 75, pp. 48–65. Springer.

Pierrehumbert, R. T. & Widnall, S. E. 1982 The two- and three-dimensional instabilities of a spatially periodic shear layer. *J. Fluid Mech.* **114**, 59–82.

Reau, N. & Tumin, A. 2002 On Harmonic perturbations in a turbulent mixing layer. *Eur. J. Mech.* B/*Fluids* **21**, 143–155.

Riley, J. J. & Metcalfe, R. W. 1980 Direct numerical simulation of a perturbed turbulent mixing layer. *AIAA Paper* 80-0274.

Rogers, M. M. & Moser, R. D. 1992 The three-dimensional evolution of a plane mixing layer: the Kelvin–Helmholtz rollup. *J. Fluid Mech.* **243**, 183–226.

Schoppa, W., Hussain, F. & Metcalfe, R. W. 1995 A new mechanism of small-scale transition in a plane mixing layer: core dynamics of spanwise vortices. *J. Fluid Mech.* **298**, 23–80.

Smyth, W. D. & Peltier, W. R. 1989 The transition between Kelvin–Helmholtz and Holmboe instability: an investigation of the overreflection hypothesis. *J. Atmos. Sci.* **46**, 3698–3720.

Stuart, J. T. 1967 On finite amplitude oscillations in laminar mixing layers. *J. Fluid Mech.* **29**, 417–440.

Tung, S. & Kleis, S. J. 1996 Initial streamwise vorticity formation in a two-stream mixing layer. *J. Fluid Mech.* **319**, 251–279.

Weisbrot, I. & Wygnanski, I. 1988 On coherent structures in a highly excited mixing layer. *J. Fluid Mech.* **195**, 137–159.

Wygnanski, I. & Petersen, R. A. 1985 Coherent motion in excited free shear flow. *AIAA Paper* 85-0539, also *AIAA J.* **25**, 201 (1987).

Wygnanski, I., Fiedler, H., Oster, D. & Dziomba, B. 1979 On the perseverance of a quasi-two-dimensional eddy structure in a turbulent mixing layer. *J. Fluid Mech.* **93**, 325–335.

Zhou, M. & Wygnanski, I. 2001 The response of a mixing layer formed between parallel streams to a concomitant excitation at two frequencies. *J. Fluid Mech.* **441**, 139–168.

Zhou, M. D., Heine, C. & Wygnanski, I. 1996 The effects of excitation on the coherent and random motion in a plane wall jet. *J. Fluid Mech.* **310**, 1–37.